

Individual-based and continuum models of phenotypically heterogeneous growing cell populations

Fiona R Macfarlane^{1,*}, Xinran Ruan², Tommaso Lorenzi^{3,*}

¹ School of Mathematics and Statistics, University of St Andrews, United Kingdom;

² School of Mathematical Sciences, Capital Normal University, 100048 Beijing, P.R. China;

³ Department of Mathematical Sciences “G. L. Lagrange”, Politecnico di Torino, 10129 Torino, Italy;

*Corresponding authors: frm3@st-andrews.ac.uk; tommaso.lorenzi@polito.it

Abstract

Existing comparative studies between individual-based models of growing cell populations and their continuum counterparts have mainly been focused on homogeneous populations, in which all cells have the same phenotypic characteristics. However, significant intercellular phenotypic variability is commonly observed in cellular systems. In light of these considerations, we develop here an individual-based model for the growth of phenotypically heterogeneous cell populations. In this model, the phenotypic state of each cell is described by a structuring variable that captures intercellular variability in cell proliferation and migration rates. The model tracks the spatial evolutionary dynamics of single cells, which undergo pressure-dependent proliferation, heritable phenotypic changes and directional movement in response to pressure differentials. We formally show that the continuum limit of this model comprises a non-local partial differential equation for the cell population density function, which generalises earlier models of growing cell populations. We report on the results of numerical simulations of the individual-based model which illustrate how proliferation-migration tradeoffs shaping the evolutionary dynamics of single cells can lead to the formation, at the population level, of travelling waves whereby highly-mobile cells locally dominate at the invasive front, while more-proliferative cells are found at the rear. Moreover, we demonstrate that there is an excellent quantitative agreement between these results and the results of numerical simulations and formal travelling-wave analysis of the continuum model, when sufficiently large cell numbers are considered. We also provide numerical evidence of scenarios in which the predictions of the two models may differ due to demographic stochasticity, which cannot be captured by the continuum model. This indicates the importance of integrating individual-based and continuum approaches when modelling the growth of phenotypically heterogeneous cell populations.

1 Introduction

Deterministic continuum models for the growth of cell populations have been increasingly used as theoretical tools to support empirical research regarding a broad spectrum of aspects of the development of solid tumours and living tissues. These models comprise partial differential equations (PDEs) that describe the evolution of cellular densities (or cell volume fractions) in response to pressure gradients that are generated by population growth, which can be mechanically-regulated [18, 76], nutrient-limited [39], pressure-dependent [14, 24, 55] or regulated by a combination of these mechanisms [10, 22, 34, 60, 71]. These models are amenable not only to numerical simulations but also to analytical approaches, which enable a complete exploration of the model parameter space. This permits a precise identification of the validity domain of the results obtained and ensures higher robustness and precision of the conclusions drawn therefrom, which ultimately provides a more in-depth theoretical understanding of the underlying cellular dynamics [53, 54].

Ideally, instead of defining such PDE models on the basis of population-scale phenomenological assumptions, one wants to derive them from first principles, that is, as the deterministic continuum limits of stochastic discrete models, *i.e.* individual-based (IB) models, which track the dynamics of single cells [4, 85]. This is to ensure that the terms comprised in the model equations provide a faithful mean-field representation of the underlying cellular dynamics. In fact, although being computationally intensive to simulate for large cell numbers and, to a wider extent, inaccessible to analytical techniques, IB models permit the representation of the finer details of cell-scale mechanisms and capture stochastic intercellular variability in the spatial and evolutionary trajectories of single cells. These aspects, which cannot be directly incorporated into phenomenological deterministic continuum models, become especially important

in scenarios where cell numbers and densities are low (*e.g.* in the early stages of embryonic development and tissue regeneration, during the formation of distant metastases upon cancer cell extravasation, and when tumour size is severely reduced after therapy), due to the stronger impact that single-cell processes and demographic stochasticity are expected to have on the dynamics of cell populations. For this reason, a range of asymptotic techniques, probabilistic methods and limiting procedures have been developed and used in previous studies to systematically derive PDE models for the growth of cell populations from their individual-based counterparts [54]. For example, reaction-diffusion and nonlinear diffusion equations have been derived from their underlying random walks [6, 19, 46, 56, 66, 69], from systems of discrete equations of motion [62, 63, 67], from discrete lattice-based exclusion processes [30, 49–51] and from cellular automata [25, 28, 79]. However, these previous studies have mainly been focused on homogeneous populations in which all cells have the same phenotypic characteristics. Such homogeneity is rarely present in cellular systems, where significant intercellular phenotypic variability is commonly observed. In light of these considerations, we develop here an IB model for the growth of phenotypically heterogeneous cell populations. In this model, every cell is viewed as an individual agent whose phenotypic state is described by a structuring variable that captures intercellular variability in cell proliferation and migration rates. Cells undergo directional movement in response to pressure differentials [3, 15, 16, 41], pressure-dependent proliferation [12, 17, 29, 76], and heritable phenotypic changes [11, 20, 44] according to a set of rules that correspond to a discrete-time branching random walk on the physical space and the space of phenotypic states [19, 21, 45]. We formally show that the deterministic continuum limit of this model is given by a non-local PDE for the cell population density function, which generalises earlier models [16, 29, 73] to the case of phenotypically heterogeneous cell populations. We then carry out numerical simulations of the IB model and compare the results obtained with the results of formal travelling-wave analysis and numerical simulations of the PDE model. The paper is organised as follows. In Section 2, we introduce the IB model. In Section 3, we present its PDE counterpart (a formal derivation is provided in Appendix A). In Section 4, in order to obtain results with broad structural stability under parameter changes, we first carry out formal travelling-wave analysis of the PDE model and then integrate the results obtained with numerical simulations of the IB model and numerical solutions of the PDE model. In Section 5, we summarise the main findings of our study and outline directions for future research.

2 The individual-based model

We model the dynamics of a phenotypically heterogeneous growing cell population. Cells within the population have the potential to undergo:

- (i) directional movement in response to pressure differentials – *i.e.* cells move down pressure gradients towards regions where they feel less compressed [3, 16, 17];
- (ii) spontaneous, heritable phenotypic changes, which lead cells to randomly transition from one phenotypic state into another [11, 20, 44];
- (iii) pressure-dependent proliferation – *i.e.* cells stop dividing, and can thus only die or remain quiescent, when the pressure that they experience overcomes a critical threshold, which is known as homeostatic pressure [9, 16, 29].

Focussing on a one-dimensional spatial domain scenario, the position of every cell at time $t \in \mathbb{R}^+$ is described by the variable $x \in \mathbb{R}$. Moreover, the phenotypic state of each cell is characterised by a structuring variable $y \in [0, Y] \subset \mathbb{R}^+$, with $Y > 0$, which takes into account intercellular variability in cell proliferation and migration rates. Here, the variable y could represent the level of expression of a gene that regulates both cell division and cell migration, such as those involved in the epithelial-to-mesenchymal transition promoting tumour invasion [2, 37, 65]. More specifically, the overexpression of some cancer-promoting genes has been shown to inhibit cell proliferation and promote cell migration in cancer cells, for example, FBXL10 expression in ovarian cancer cell lines [89] and EphB2 expression in glioblastomas [87]. Similarly, the downregulation of miR-451 observed in glioblastomas has been shown to reduce the proliferation rate and increase the migration potential of the cells [40].

Therefore in the model, without loss of generality, we consider the case where larger values of y correlate with a higher cell migration rate but a lower proliferation rate due to proliferation-migration tradeoffs [1, 2, 33, 35–38, 42, 68, 74].

We discretise the time, space and phenotype variables via

$$t_k = k\tau \in \mathbb{R}^+, \quad x_i = i\chi \in \mathbb{R} \quad \text{and} \quad y_j = j\eta \in [0, Y] \quad \text{with} \quad k, j \in \mathbb{N}_0, \quad i \in \mathbb{Z}, \quad \tau, \chi, \eta \in \mathbb{R}_*^+.$$

Here τ , χ and η are the time-, space- and phenotype-step, respectively. We represent every single cell as an agent that occupies a position on the lattice $\{x_i\}_{i \in \mathbb{Z}} \times \{y_j\}_{j \in \mathbb{N}_0}$, and we introduce the dependent variable $N_{i,j}^k \in \mathbb{N}_0$ to model the number of cells in the phenotypic state y_j at position x_i at time t_k . The cell population density and the corresponding cell density are defined, respectively, as follows

$$n_{i,j}^k \equiv n(t_k, x_i, y_j) := \frac{N_{i,j}^k}{\chi\eta} \quad \text{and} \quad \rho_i^k \equiv \rho(t_k, x_i) := \eta \sum_j n_{i,j}^k. \quad (2.1)$$

We further define the pressure experienced by the cells (*i.e.* the cell pressure) as a function of the cell density through the following barotropic relation

$$p_i^k \equiv p(t_k, x_i) = \Pi(\rho_i^k), \quad (2.2)$$

where the function Π satisfies the following assumptions [16, 73, 84]

$$\Pi(0) = 0, \quad \frac{d}{d\rho} \Pi(\rho) \geq 0 \quad \text{for } \rho \in \mathbb{R}_*^+. \quad (2.3)$$

As summarised by the schematics in Figure 1, between time-steps k and $k+1$, each cell in phenotypic state $y_j \in (0, Y)$ at position $x_i \in \mathbb{R}$ can first move, next undergo phenotypic changes and then die or divide according to the rules described in the following subsections.

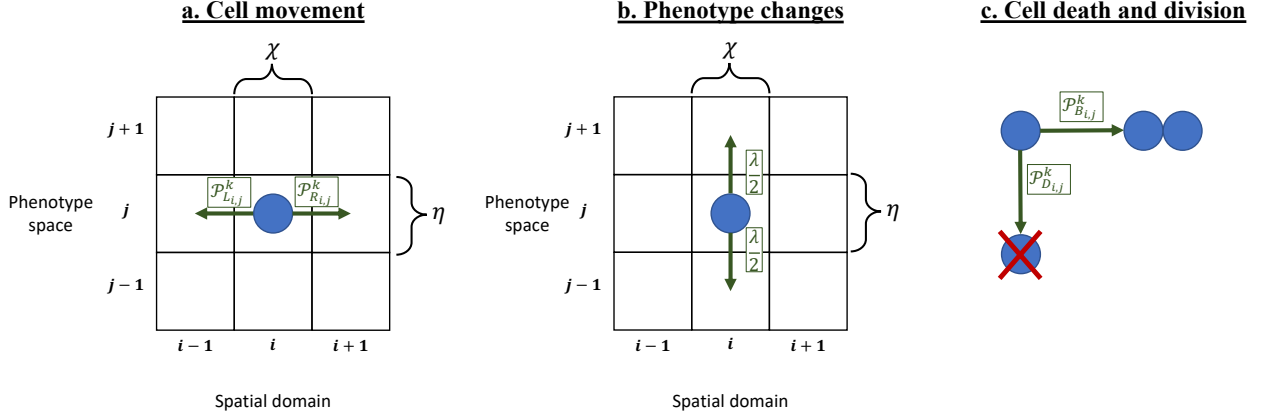


Figure 1: Schematics summarising the rules that govern the spatial evolutionary dynamics of single cells in the IB model. Between time-steps k and $k+1$, each cell in phenotypic state $y_j \in (0, Y)$ at position $x_i \in \mathbb{R}$ may: **a.** move to either of the positions x_{i-1} and x_{i+1} with probabilities $\mathcal{P}_{L,i,j}^k$ and $\mathcal{P}_{R,i,j}^k$ defined via (2.12) and (2.13); **b.** undergo a phenotypic change and thus enter into either of the phenotypic states y_{j-1} and y_{j+1} with probabilities $\lambda/2$; **c.** die or divide with probabilities $\mathcal{P}_{D,i,j}^k$ and $\mathcal{P}_{B,i,j}^k$ defined via (2.4) and (2.5).

2.1 Mathematical modelling of cell death and division

To incorporate the effects of cell proliferation, we assume that a dividing cell is instantly replaced by two identical cells that inherit the phenotypic state of the parent cell (*i.e.* the progenies are placed on the same lattice site as their parent), while a dying cell is instantly removed from the population. We model pressure-dependent proliferation by letting the cells divide, die or remain quiescent with probabilities that depend on their phenotypic states and the pressure that they experience. In particular, to define the probabilities of cell division and death, we introduce the function $R(y_j, p_i^k)$, which describes the net growth rate of the cell population density at position x_i at time t_k , and assume that between time-steps k and $k+1$ a cell in phenotypic state y_j at position x_i may die with probability

$$\mathcal{P}_{D,i,j}^k := \tau R(y_j, p_i^k)_- \quad \text{where} \quad R(y_j, p_i^k)_- = -\min(0, R(y_j, p_i^k)), \quad (2.4)$$

divide with probability

$$\mathcal{P}_{B,i,j}^k := \tau R(y_j, p_i^k)_+ \quad \text{where} \quad R(y_j, p_i^k)_+ = \max(0, R(y_j, p_i^k)) \quad (2.5)$$

or remain quiescent (*i.e.* do not divide nor die) with probability

$$\mathcal{P}_{Q_{i,j}}^k := 1 - \mathcal{P}_{B_{i,j}}^k - \mathcal{P}_{D_{i,j}}^k. \quad (2.6)$$

Note that we are implicitly assuming the time-step τ to be sufficiently small that $0 < \mathcal{P}_{B_{i,j}}^k + \mathcal{P}_{D_{i,j}}^k < 1$ for all values of i, j and k .

In order to capture the fact that, as mentioned earlier, larger values of y_j correlate with a lower cell proliferation rate, along with the fact that cells will stop dividing if the pressure at their current position becomes larger than the homeostatic pressure, which we model by means of the parameter $p_M > 0$, we make the following assumptions

$$R(Y, 0) = 0, \quad R(0, p_M) = 0, \quad \partial_p R(y, p) < 0 \quad \text{and} \quad \partial_y R(y, p) < 0 \quad \text{for } (y, p) \in (0, Y) \times \mathbb{R}^+. \quad (2.7)$$

In particular, we will focus on the case where

$$R(y, p) := r(y) - \frac{p}{p_M} \quad \text{with} \quad r(Y) = 0, \quad r(0) = 1, \quad \frac{d}{dy} r(y) < 0 \quad \text{for } y \in (0, Y). \quad (2.8)$$

Remark 1. Under assumptions (2.7), definitions (2.5)-(2.6) ensure that if $p_i^k \geq p_M$ then every cell at position x_i can only die or remain quiescent between time-steps k and $k + 1$. Hence, in the remainder of the paper we will let the following condition hold

$$\max_{i \in \mathbb{Z}} p_i^0 \leq p_M \quad (2.9)$$

so that

$$p_i^k \leq p_M \quad \text{for all } (k, i) \in \mathbb{N}_0 \times \mathbb{Z}. \quad (2.10)$$

2.2 Mathematical modelling of phenotypic changes

We take into account heritable phenotypic changes by allowing cells to update their phenotypic states according to a random walk along the phenotypic dimension. More precisely, between time-steps k and $k + 1$, every cell either enters a new phenotypic state, with probability $\lambda \in [0, 1]$, or remains in its current phenotypic state, with probability $1 - \lambda$. Since, as mentioned earlier, we consider only spontaneous phenotypic changes that occur randomly due to non-genetic instability, we assume that a cell in phenotypic state y_j that undergoes a phenotypic change enters into either of the phenotypic states $y_{j \pm 1} = y_j \pm \eta$ with probabilities $\lambda/2$. No-flux boundary conditions are implemented by aborting any attempted phenotypic variation of a cell if it requires moving into a phenotypic state outside the interval $[0, Y]$.

2.3 Mathematical modelling of cell movement

We model directional cell movement in response to pressure differentials as a biased random walk along the spatial dimension, whereby the movement probabilities depend on the difference between the pressure at the position occupied by a cell and the pressure at the neighbouring positions. As mentioned earlier, we consider the case where larger values of y_j correlate with a higher cell migration rate. Hence, we modulate the probabilities of cell movement by the function $\mu(y_j)$, which provides a measure of the mobility of cells in phenotypic state y_j and thus satisfies the following assumptions

$$\mu(0) > 0, \quad \frac{d}{dy} \mu(y) > 0 \quad \text{for } y \in (0, Y]. \quad (2.11)$$

Then we assume that between time-steps k and $k + 1$ a cell in phenotypic state y_j at position x_i may move to the position $x_{i-1} = x_i - \chi$ (*i.e.* move left) with probability

$$\mathcal{P}_{L_{i,j}}^k = \nu \mu(y_j) \frac{(p_i^k - p_{i-1}^k)_+}{2p_M} \quad \text{where} \quad (p_i^k - p_{i-1}^k)_+ = \max(0, p_i^k - p_{i-1}^k), \quad (2.12)$$

move to the position $x_{i+1} = x_i + \chi$ (*i.e.* move right) with probability

$$\mathcal{P}_{R_{i,j}}^k = \nu \mu(y_j) \frac{(p_i^k - p_{i+1}^k)_+}{2p_M} \quad \text{where} \quad (p_i^k - p_{i+1}^k)_+ = \max(0, p_i^k - p_{i+1}^k) \quad (2.13)$$

or remain stationary (*i.e.* do not move left nor right) with probability

$$\mathcal{P}_{S_{i,j}}^k = 1 - \mathcal{P}_{L_{i,j}}^k - \mathcal{P}_{R_{i,j}}^k. \quad (2.14)$$

Here, the parameter $\nu > 0$ is a scaling factor, which we implicitly assume to be sufficiently small that $0 < \nu \mu(y_j) < 1$ for all $y_j \in [0, Y]$. Under condition (2.9), this assumption on ν along with the a priori estimate (2.10) implies that definitions (2.12) and (2.13) are such that $0 < \mathcal{P}_{L_{i,j}}^k + \mathcal{P}_{R_{i,j}}^k < 1$ for all values of i, j and k .

Remark 2. Definitions (2.12) and (2.13) ensure that cells will move down pressure gradients so as to reach regions where they feel less compressed.

3 The corresponding continuum model

Through a method analogous to those that we previously employed in [5, 13, 19, 61, 82], letting the time-step $\tau \rightarrow 0$, the space-step $\chi \rightarrow 0$ and the phenotype-step $\eta \rightarrow 0$ in such a way that

$$\frac{\nu \chi^2}{2\tau} \rightarrow \alpha \in \mathbb{R}_*^+ \quad \text{and} \quad \frac{\lambda \eta^2}{2\tau} \rightarrow \beta \in \mathbb{R}_*^+, \quad (3.1)$$

one can formally show (see Appendix A) that the deterministic continuum counterpart of the stochastic discrete model presented in Section 2 is given by the following non-local PDE for the cell population density function $n(t, x, y)$

$$\begin{cases} \partial_t n - \alpha \hat{\mu}(y) \partial_x (n \partial_x p) = R(y, p) n + \beta \partial_{yy}^2 n, & (x, y) \in \mathbb{R} \times (0, Y) \\ p = \Pi(\rho), \quad \rho := \int_0^Y n(t, x, y) dy, \end{cases} \quad (3.2)$$

where $\hat{\mu}(y) := \frac{\mu(y)}{p_M}$. The non-local PDE (3.2) is subject to zero Neumann (*i.e.* no-flux) boundary conditions at $y = 0$ and $y = Y$, as well as to an initial condition such that the continuum analogue of condition (2.9) holds, that is,

$$\max_{x \in \mathbb{R}} p(0, x) \leq p_M. \quad (3.3)$$

The mathematical model defined by complementing (3.2) with assumptions (2.3), (2.7) and (2.11) generalises earlier models of pressure-dependent cell population growth [16, 29, 73] to the case of phenotypically heterogeneous cell populations.

4 Main results

In this section, we first present the result of formal travelling-wave analysis of the PDE model (Subsection 4.1) and then integrate these results with numerical simulations of the IB model and numerical solutions of the PDE model (Subsection 4.2).

4.1 Formal travelling-wave analysis

We focus on a biological scenario in which cell movement occurs on a slower timescale compared to cell division and death, while spontaneous, heritable phenotypic changes occur on a slower timescale compared to cell movement [44, 81]. To this end, we introduce a small parameter $\varepsilon > 0$ and let

$$\alpha := \varepsilon, \quad \beta := \varepsilon^2. \quad (4.1)$$

Moreover, in order to explore the long-time behaviour of the cell population (*i.e.* the behaviour of the population over many cell generations), we use the time scaling $t \rightarrow \frac{t}{\varepsilon}$ in (3.2). Taken together, this gives the following non-local PDE

for the cell population density function $n_\varepsilon(t, x, y) = n(\frac{t}{\varepsilon}, x, y)$

$$\begin{cases} \varepsilon \partial_t n_\varepsilon - \varepsilon \hat{\mu}(y) \partial_x (n_\varepsilon \partial_x p_\varepsilon) = R(y, p_\varepsilon) n_\varepsilon + \varepsilon^2 \partial_{yy}^2 n_\varepsilon, & (x, y) \in \mathbb{R} \times (0, Y) \\ p_\varepsilon = \Pi(\rho_\varepsilon), \quad \rho_\varepsilon := \int_0^Y n_\varepsilon(t, x, y) dy. \end{cases} \quad (4.2)$$

Using a method analogous to those that we have previously employed in [57, 58], denoting by $\delta_{(\cdot)}(y)$ the Dirac delta centred at $y = (\cdot)$, one can formally show (see Appendix B) that, under assumptions (2.3), (2.8) and (2.11), as $\varepsilon \rightarrow 0$, the non-local PDE (4.2) admits travelling-wave solutions of the form

$$n_\varepsilon(z, y) \approx \rho(z) \delta_{\bar{y}(z)}(y), \quad z = x - ct, \quad c \in \mathbb{R}_*^+, \quad (4.3)$$

where $\bar{y}(z)$ is the unique maximum point of the solution to the following equation

$$-(c + \hat{\mu}(y)p') \partial_z u = \left(r(y) - \frac{p}{p_M} \right) + (\partial_y u)^2, \quad u \equiv u(z, y), \quad (z, y) \in \mathbb{R} \times (0, Y)$$

subject to the constraint $\max_{y \in [0, Y]} u(z, y) = u(z, \bar{y}(z)) = 0$ for $z \in \text{Supp}(\rho)$, and the cell density $\rho(z)$ is such that the pressure $p(z) = \Pi(\rho(z))$ satisfies the following relation

$$p(z) = p_M r(\bar{y}(z)) \quad z \in \text{Supp}(p), \quad (4.4)$$

provided that the wave speed c satisfies the following necessary condition

$$c \geq \sup_{z \in \text{Supp}(r(\bar{y}))} 2 \left| \frac{d}{dy} r(\bar{y}(z)) \right| \sqrt{\frac{\mu(\bar{y}(z))}{|\partial_{yy}^2 u(z, \bar{y}(z))|}}. \quad (4.5)$$

Moreover,

$$\text{Supp}(p) = (-\infty, \ell) \quad \text{with } \ell \in \mathbb{R} \text{ such that } \bar{y}(\ell) = Y \quad (4.6)$$

and

$$\lim_{z \rightarrow -\infty} \bar{y}(z) = 0, \quad \lim_{z \rightarrow -\infty} p(z) = p_M, \quad \bar{y}'(z) > 0 \text{ and } p'(z) < 0 \quad z \in (-\infty, \ell). \quad (4.7)$$

From a biological point of view, $\bar{y}(z)$ represents the dominant phenotype of cells at a certain position along the invading wave $p(z)$. Since larger values of y correlate with a lower proliferation rate and a higher migration rate, the fact that $\bar{y}(z)$ increases monotonically from 0 to Y while $p(z)$ decreases monotonically from p_M to 0 (cf. the results given by (4.6) and (4.7)) provides a mathematical formalisation of the idea that spatial sorting causes cells with a more mobile/less proliferative phenotype to become concentrated towards the front of the invading wave, which is thus a sparsely populated region, whereas phenotypic selection leads cells with a less mobile/more proliferative phenotype to dominate at the rear, which is then a densely populated region.

4.2 Numerical simulations

4.2.1 Set-up of numerical simulations

In order to carry out numerical simulations, we consider the time interval $[0, T]$, with $T = 8$, we restrict the physical domain to the closed interval $[0, X]$, with $X = 25$, and choose $Y = 1$. In order to facilitate the integration between numerical simulations and the results of formal travelling-wave analysis presented in Subsection 4.1, we solve numerically the rescaled PDE model (4.2), with $\varepsilon = 0.01$, and we carry out numerical simulations of the scaled IB model obtained by introducing the time scaling $t_k \rightarrow \frac{t_k}{\varepsilon} = k \frac{\tau}{\varepsilon}$ and reformulating the governing rules of cell dynamics that are detailed in Section 2 in terms of

$$p_{\varepsilon i}^k \equiv p_\varepsilon(t_k, x_i) = p\left(\frac{t_k}{\varepsilon}, x_i\right) = \Pi(\rho_{\varepsilon i}^k),$$

with

$$\rho_{\varepsilon i}^k \equiv \rho_\varepsilon(t_k, x_i) = \rho\left(\frac{t_k}{\varepsilon}, x_i\right) := \eta \sum_j n_{\varepsilon i, j}^k \quad \text{and} \quad n_{\varepsilon i, j}^k \equiv n_\varepsilon\left(\frac{t_k}{\varepsilon}, x_i, y_j\right) = n\left(\frac{t_k}{\varepsilon}, x_i, y_j\right) := \frac{N_{\varepsilon i, j}^k}{\chi \eta}.$$

Moreover, we choose $\tau = 5 \times 10^{-5}$, $\chi = 0.01$ and $\eta = 0.02$, and then set $\nu = \frac{2\tau}{\chi^2}\varepsilon$ and $\lambda = \frac{2\tau}{\eta^2}\varepsilon^2$ in order to ensure that conditions (3.1) and (4.1) are simultaneously satisfied.

We consider a biological scenario in which, initially, the cell population is localised along the $x = 0$ boundary and most of the cells are in the phenotypic state $y = \bar{y}^0$ at every position. Specifically, we implement the following initial cell distribution for the IB model

$$N_{ei,j}^0 = \text{int}(F_\varepsilon(x_i, y_j)) \quad \text{with} \quad F_\varepsilon(x, y) = A_0 C e^{-x^2} e^{-\frac{(y-\bar{y}^0)^2}{\varepsilon}}, \quad (4.8)$$

where $\text{int}(\cdot)$ is the integer part of (\cdot) and C is a normalisation constant such that

$$C \int_0^Y e^{-\frac{(y-\bar{y}^0)^2}{\varepsilon}} dy = 1.$$

Unless otherwise specified, we choose $A_0 = 10$ and $\bar{y}^0 = 0.2$, that is, the initially dominant phenotype of the cell population is $y = 0.2$. The initial cell density and pressure are then calculated via (2.1) and (2.2). The initial cell population density function $n_\varepsilon(0, x, y) = n_\varepsilon^0(x, y)$, is defined as a suitable continuum analogue of the cell population density $n_{ei,j}^0 := \frac{N_{ei,j}^0}{\chi\eta}$, with $N_{ei,j}^0$ given by (4.8). Specifically, we set

$$n_\varepsilon^0(x, y) := \left(\frac{F_\varepsilon(x, y)}{\chi\eta} - \frac{1.5}{\chi\eta} \right)_+,$$

where $F_\varepsilon(x, y)$ is defined via (4.8) and $(\cdot)_+$ is the positive part of (\cdot) .

We define $R(y, p_\varepsilon)$ via (2.8) and, having chosen $Y = 1$, we further define

$$r(y) := 1 - y^2 \quad \text{and} \quad \mu(y) := 0.01 + y^2$$

so as to ensure that assumptions (2.7), (2.8) and (2.11) are satisfied. Moreover, we investigate the following three definitions of the barotropic relation for the cell pressure, all satisfying assumptions (2.3):

$$p_\varepsilon = \Pi(\rho_\varepsilon) := \begin{cases} \rho_\varepsilon & \text{(Case 1)} \\ K_\gamma (\rho_\varepsilon)^\gamma & \text{with } K_\gamma > 0, \gamma > 1 \quad \text{(Case 2)} \\ \kappa (\rho_\varepsilon - \rho^*)_+ & \text{with } \kappa, \rho^* > 0 \quad \text{(Case 3).} \end{cases} \quad (4.9)$$

The definition given by Case 1 corresponds to the simplified scenario in which the cell pressure is a linear function of the cell density. In the definition given by Case 2, which was proposed in [73], the parameter K_γ is a scaling factor and the parameter γ provides a measure of the stiffness of the barotropic relation (*i.e.* the limit $\gamma \rightarrow \infty$ corresponds to the scenario in which cells behave like an incompressible fluid). In the definition given by Case 3, which is such that the cell pressure is zero for $\rho \leq \rho^*$ and is a monotonically increasing function of the cell density for $\rho > \rho^*$, the parameter κ is a scaling factor and ρ^* is the density below which the force that the cells exert upon one another is negligible [29, 84]. Unless otherwise specified: when the cell pressure is defined via Case 1 we choose $p_M = 4.95 \times 10^4$; when the cell pressure is defined via Case 2 we choose $p_M = 3.675 \times 10^9$, $\gamma = 2$ and $K_\gamma = \frac{3}{2}$; when the cell pressure is defined via Case 3 we choose $p_M = 4.94 \times 10^5$, $\kappa = 10$ and $\rho^* = 10^2$.

Remark 3. *The initial conditions and the values of p_M that are considered here are such that conditions (2.9) and (3.3) are satisfied.*

4.2.2 Computational implementation of the IB model

All simulations are performed in `MATLAB`. At each time-step, each cell undergoes a three-phase process: (i) cell movement, according to the probabilities defined via (2.12)-(2.14); (ii) phenotypic changes, with probabilities $\lambda/2$; (iii) division and death, according to the probabilities defined via (2.5)-(2.6). For each cell, during each phase, a random number is drawn from the standard uniform distribution on the interval $(0, 1)$ using the built-in `MATLAB` function `RAND`. It is then evaluated whether this number is lower than the probability of the event occurring and if so the event occurs. Since $x_i \in [0, X]$, the attempted movement of a cell is aborted if it requires moving out of the spatial domain.

4.2.3 Methods used to solve numerically the non-local PDE (4.2)

Full details of the methods used to solve numerically the non-local PDE (4.2) posed on $(0, T] \times (0, X) \times (0, Y)$ and subject to suitable initial and boundary conditions are given in Appendix C.

4.2.4 Results of numerical simulations

Formation of complex spatial patterns of population growth. The plots in the top lines of Figures 2-4 summarise the results of numerical simulations of the IB model for the barotropic relations given by Cases 1-3 in (4.9). We plot in the left panels the scaled cell population density, $n_\varepsilon/\rho_\varepsilon$, and in the right panels (solid blue lines) the scaled cell pressure, p_ε/p_M , at progressive times.

The results of numerical simulations under all three cases display very similar dynamics, both with respect to the cell population density and the cell pressure, where we observe evolution to travelling-wave profiles of almost identical shapes and speeds (see also Remark 4). The incorporation of proliferation-migration tradeoffs lead cells to be non-uniformly distributed across both physical and phenotype space. More precisely, we observe a relatively small subpopulation of highly-mobile but minimally-proliferative cells (*i.e.* cells in phenotypic states $y \approx Y$) that becomes concentrated towards the front of the invading wave, while rapidly-proliferating but minimally-mobile cells (*i.e.* cells in phenotypic states $y \approx 0$) make up the bulk of the population in the rear. This is due to a dynamic interplay between spatial sorting and phenotypic selection. In fact, a more efficient response to pressure differentials by more-mobile cells leads to their positioning at the front of the wave, where the pressure is lower, before being overcome by the more-proliferative cells encroaching from the rear of the wave, which are ultimately selected due to their higher proliferative potential.

Quantitative agreement between the IB model and its PDE counterpart. The plots in the bottom lines of Figures 2-4 summarise the corresponding numerical solutions of the PDE model (4.2). Comparing these plots with those in the top lines, we can see that there is an excellent quantitative agreement between the results of numerical simulations of the IB model and the numerical solutions of its PDE counterpart, both with respect to the cell population density and the cell pressure, for each of the barotropic relations given by Cases 1-3 in (4.9).

All these plots indicate that, in agreement with the results presented in Subsection 4.1 (cf. the results given by (4.3)), when ε is sufficiently small, the scaled cell population density $n_\varepsilon/\rho_\varepsilon$ is concentrated as a sharp Gaussian with maximum at a single point $\bar{y}_\varepsilon(t, x)$ for all $x \in \text{Supp}(p_\varepsilon)$. The maximum point $\bar{y}_\varepsilon(t, x)$ corresponds to the dominant phenotype within the cell population at position x and time t . Again in agreement with the results presented in Subsection 4.1 (cf. the results given by (4.6) and (4.7)), the cell pressure p_ε behaves like a one-sided compactly supported and monotonically decreasing travelling front that connects p_M to 0, while the dominant phenotype \bar{y}_ε increases monotonically from $y = 0$ to $y = Y$ across the support of the invading wave. Moreover, we find an excellent quantitative agreement between $p_\varepsilon(t, x)/p_M$ and $r(\bar{y}_\varepsilon(t, x))$ (cf. the solid blue and dashed cyan lines in the right panels of Figures 2-4). This indicates that, when ε is sufficiently small, relation (4.4) is satisfied as well.

In order to measure the speed of these travelling waves, we track the dynamics of the points $x_{\varepsilon 1}(t)$, $x_{\varepsilon 2}(t)$ and $x_{\varepsilon 3}(t)$ such that

$$p_\varepsilon(t, x_{\varepsilon 1}(t)) = 0.2p_M, \quad p_\varepsilon(t, x_{\varepsilon 2}(t)) = 0.5p_M, \quad p_\varepsilon(t, x_{\varepsilon 3}(t)) = 0.8p_M. \quad (4.10)$$

Notably, we observe the evolution of $x_{\varepsilon 1}(t)$, $x_{\varepsilon 2}(t)$ and $x_{\varepsilon 3}(t)$ towards straight lines of approximatively the same slope ≈ 2.5 (see the insets of the right panels in Figures 2-4). Moreover, an equivalent tracking of $\tilde{x}_{\varepsilon 1}(t)$, $\tilde{x}_{\varepsilon 2}(t)$ and $\tilde{x}_{\varepsilon 3}(t)$ such that $\bar{y}_\varepsilon(t, \tilde{x}_{\varepsilon 1}(t)) = 0.2$, $\bar{y}_\varepsilon(t, \tilde{x}_{\varepsilon 2}(t)) = 0.5$ and $\bar{y}_\varepsilon(t, \tilde{x}_{\varepsilon 3}(t)) = 0.8$, with

$$\bar{y}_\varepsilon(t, x) := \arg \max_{y \in [0, Y]} n_\varepsilon(t, x, y), \quad (4.11)$$

yields quasi-identical results (results not shown). This supports the idea that p_ε behaves like a travelling front of speed $c \approx 2.5$. Such a value of the speed is coherent with the condition on the minimal wave speed given by (4.5). In fact, inserting into (4.5) the numerical values of $\bar{y}_\varepsilon(8, x)$ in place of $\bar{y}(z)$ and the numerical values of $\partial_{yy}^2 u_\varepsilon(8, x, \bar{y}_\varepsilon(8, x))$ with $u_\varepsilon = \varepsilon \log(n_\varepsilon)$ in place of $\partial_{yy}^2 u(z, \bar{y}(z))$ gives $c \gtrsim 2.5$.

Remark 4. *The robustness of the results of numerical simulations of the IB model presented so far is supported by the fact that there is an excellent quantitative agreement between them and the results of numerical simulations and formal travelling-wave analysis of the corresponding PDE model. In fact, in the light of this agreement, independently of the*

specific definitions of the model functions Π , R and μ , provided that assumptions (2.3), (2.7) and (2.11) are satisfied, and sufficiently large cell numbers are considered, in the asymptotic regime $\varepsilon \rightarrow 0$, one can expect the rules governing the spatial evolutionary dynamics of single cells considered here to bring about patterns of population growth that will ultimately be qualitatively similar to those of Figures 2-4.

Case 1

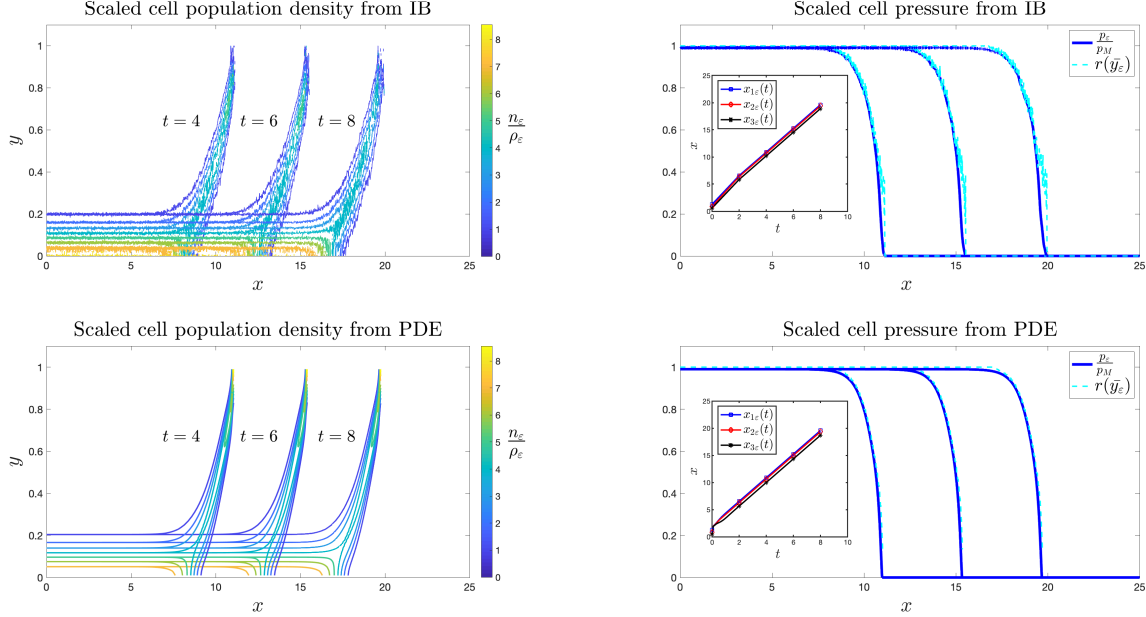


Figure 2: Numerical simulation results of the IB model (top row) and the PDE model (4.2) (bottom row) in the case where the cell pressure is defined through the barotropic relation given by Case 1 in (4.9). Plots display the scaled cell population density $n_\varepsilon/\rho_\varepsilon$ (left panels) and the scaled cell pressure p_ε/p_M (right panels, solid blue lines) at three successive time instants (*i.e.* $t = 4$, $t = 6$ and $t = 8$) for both modelling approaches. The dashed cyan lines in the right panels highlight the corresponding values of $r(\bar{y}_\varepsilon)$, with \bar{y}_ε defined via (4.11). The insets of the right panels display the plots of $x_{\varepsilon 1}(t)$ (blue squares), $x_{\varepsilon 2}(t)$ (red diamonds) and $x_{\varepsilon 3}(t)$ (black stars) defined via (4.10). The results from the IB model were obtained by averaging over 10 simulations.

Possible discrepancies between the IB model and its PDE counterpart. In the cases discussed so far, we have observed excellent quantitative agreement between averaged results of numerical simulations of the IB model and numerical solutions of the corresponding PDE model. However, we hypothesise that possible differences between the two models can emerge when cell dynamics are strongly impacted by demographic stochasticity, which cannot be captured by the PDE model.

In general, we expect demographic stochasticity to have a stronger impact on cell dynamics in the presence of smaller values of the homeostatic pressure p_M , since smaller values of p_M correlate with smaller cell numbers. Moreover, in the case where cells are initially distributed across both physical and phenotype space according to (4.8), we expect demographic stochasticity to escalate during the early stages of cell dynamics if sufficiently small values of the parameter A_0 and sufficiently large values of the parameter \bar{y}^0 (*i.e.* values of \bar{y}^0 sufficiently far from 0 and sufficiently close to Y) are considered. In fact, smaller values of A_0 correlate with lower initial cell numbers. Moreover, since cells in phenotypic states $y \approx 0$ will ultimately be selected in the rear of the invading wave (cf. the plots in the left panels of Figures 2-4), bottleneck effects leading to a temporary drastic reduction in the size of the cell population may occur if \bar{y}^0 is sufficiently far from 0.

Hence, to test the aforementioned hypothesis, we carry out numerical simulations of the two models for decreasing values of A_0 and increasing values of \bar{y}^0 in the initial cell distribution (4.8). Furthermore, we define the cell pressure through the barotropic relation given by Case 1 in (4.9) and set $p_M := \max_{x \in [0, X]} \Pi(\rho_\varepsilon(0, x))$, so that smaller values of A_0

Case 2

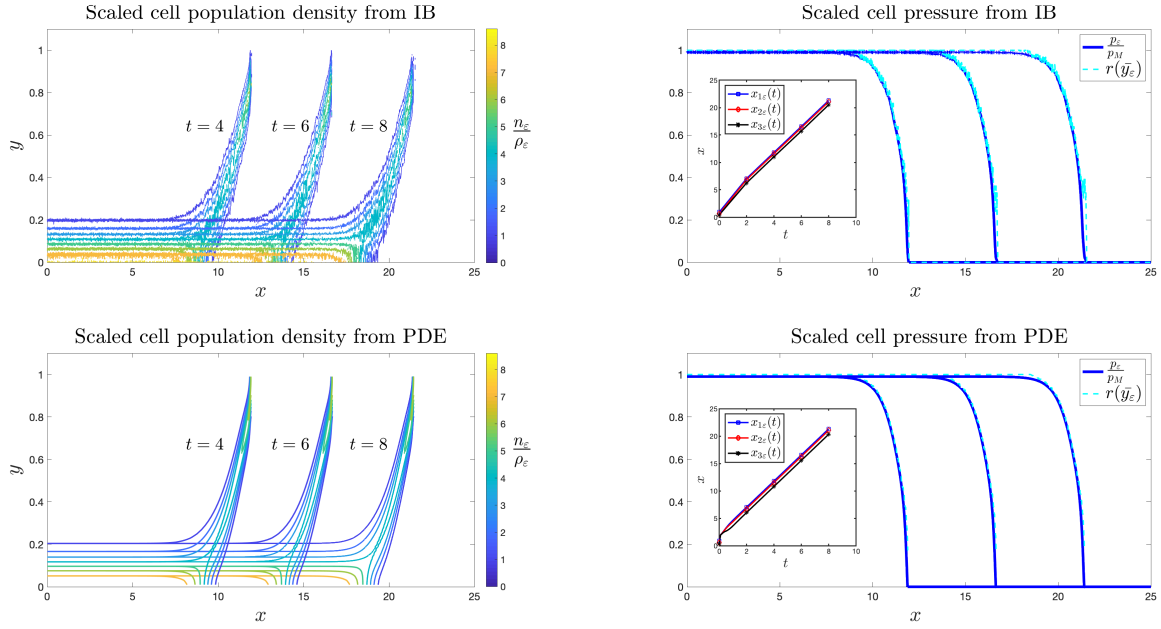


Figure 3: Numerical simulation results of the IB model (top row) and the PDE model (4.2) (bottom row) in the case where the cell pressure is defined through the barotropic relation given by Case 2 in (4.9). Plots display the scaled cell population density $n_\varepsilon/\rho_\varepsilon$ (left panels) and the scaled cell pressure p_ε/p_M (right panels, solid blue lines) at three successive time instants (*i.e.* $t = 4$, $t = 6$ and $t = 8$) for both modelling approaches. The dashed cyan lines in the right panels highlight the corresponding values of $r(\bar{y}_\varepsilon)$, with \bar{y}_ε defined via (4.11). The insets of the right-hand panels display the plots of $x_{\varepsilon 1}(t)$ (blue squares), $x_{\varepsilon 2}(t)$ (red diamonds) and $x_{\varepsilon 3}(t)$ (black stars) defined via (4.10). The results from the IB model were obtained by averaging over 10 simulations.

Case 3

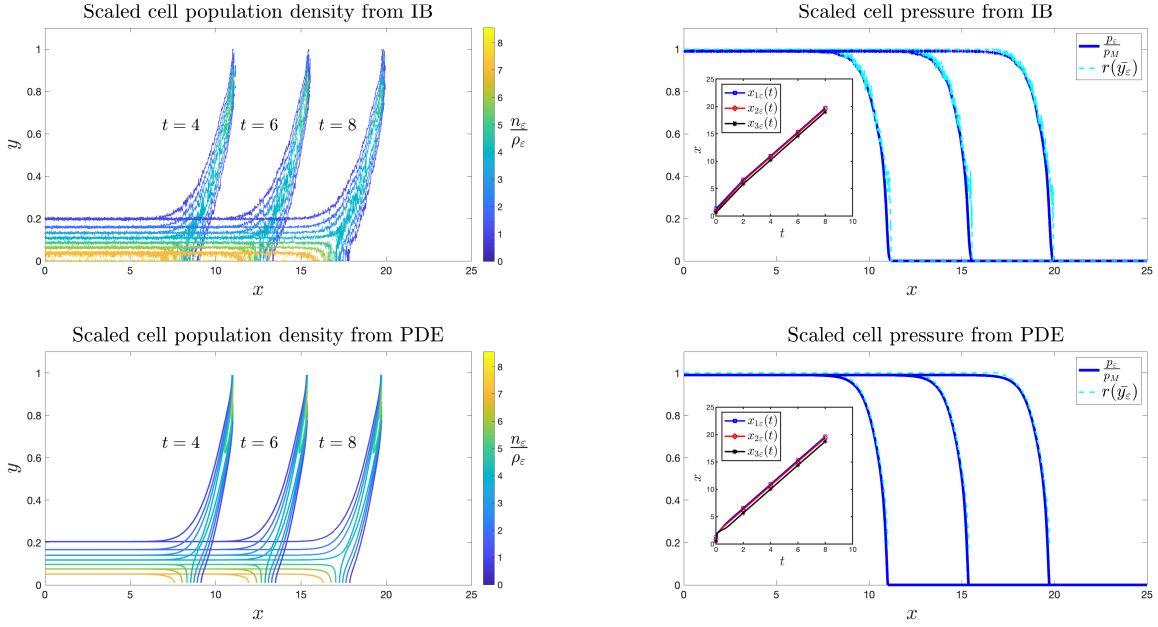


Figure 4: Numerical simulation results of the IB model (top row) and the PDE model (4.2) (bottom row) in the case where the cell pressure is defined through the barotropic relation given by Case 3 in (4.9). Plots display the scaled cell population density $n_\varepsilon/\rho_\varepsilon$ (left panels) and the scaled cell pressure p_ε/p_M (right panels, solid blue lines) at three successive time instants (*i.e.* $t = 4$, $t = 6$ and $t = 8$) for both modelling approaches. The dashed cyan lines in the right panels highlight the corresponding values of $r(\bar{y}_\varepsilon)$, with \bar{y}_ε defined via (4.11). The insets of the right-hand panels display the plots of $x_{\varepsilon 1}(t)$ (blue squares), $x_{\varepsilon 2}(t)$ (red diamonds) and $x_{\varepsilon 3}(t)$ (black stars) defined via (4.10). The results from the IB model were obtained by averaging over 10 simulations.

correspond to smaller value of p_M as well.

The results obtained for the IB model are summarised by the plots in Figure 5, which display typical dynamics of the scaled cell pressure p_ε/p_M , while the corresponding results for the PDE model (4.2) are summarised by the plots in Figure 6. These results corroborate our hypothesis by demonstrating that the quantitative agreement between the IB model and its PDE counterpart deteriorates when smaller values of A_0 and larger values of \bar{y}^0 are considered (cf. the plots in the bottom-line panels of Figures 5 and 6).

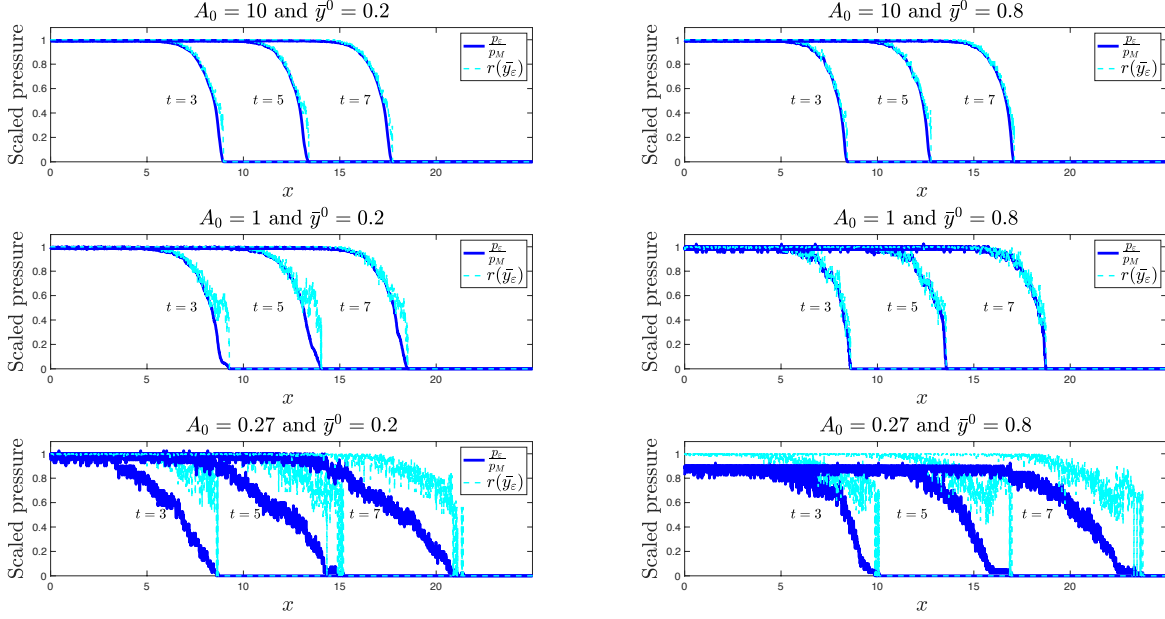


Figure 5: Numerical simulation results of the IB model for different values of the parameters A_0 and \bar{y}^0 in the initial cell distribution (4.8) – *i.e.* $\bar{y}^0 = 0.2$ (left column) or $\bar{y}^0 = 0.8$ (right column) and $A_0 = 10$ (top row) or $A_0 = 1$ (central row) or $A_0 = 0.27$ (bottom row). The solid blue lines highlight the values of the scaled cell pressure p_ε/p_M at three successive time instants (*i.e.* $t = 3, t = 5$ and $t = 7$). The dashed cyan lines highlight the corresponding values of $r(\bar{y}_\varepsilon)$, with \bar{y}_ε defined via (4.11). These results were obtained by averaging over 10 simulations.

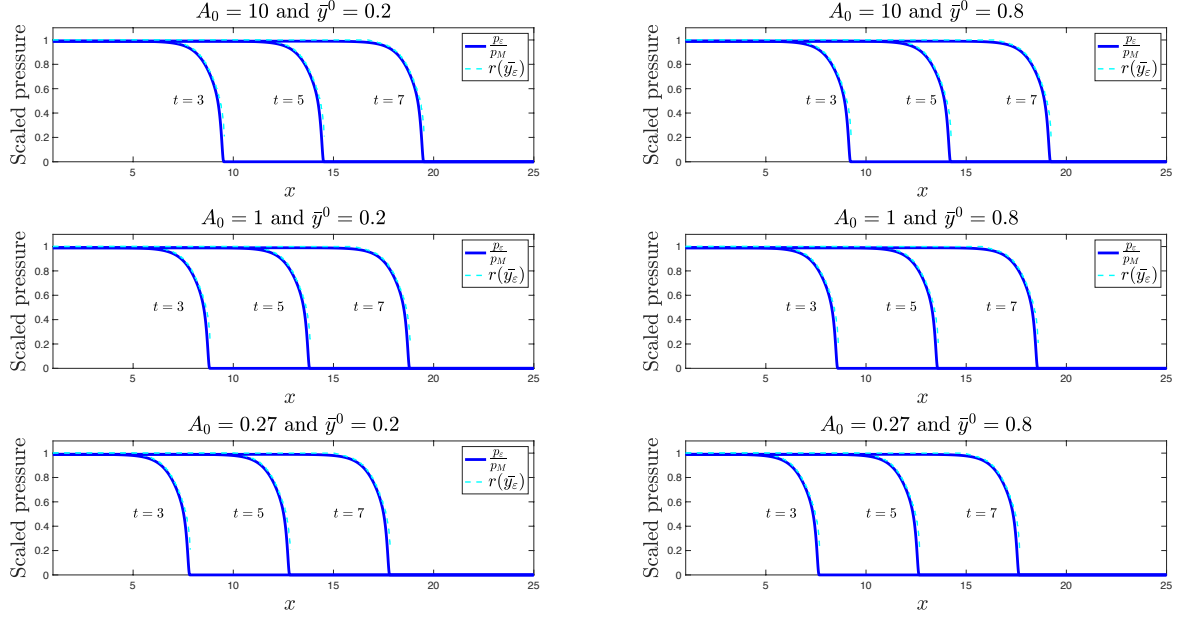


Figure 6: Numerical simulation results of the PDE model (4.2) for different values of the parameters A_0 and \bar{y}^0 in the initial cell distribution (4.8) – *i.e.* $\bar{y}^0 = 0.2$ (left column) or $\bar{y}^0 = 0.8$ (right column) and $A_0 = 10$ (top row) or $A_0 = 1$ (central row) or $A_0 = 0.27$ (bottom row). The solid blue lines highlight the values of the scaled cell pressure p_ε/p_M at three successive time instants (*i.e.* $t = 3, t = 5$ and $t = 7$). The dashed cyan lines highlight the corresponding values of $r(\bar{y}_\varepsilon)$, with \bar{y}_ε defined via (4.11).

In line with our expectations, this is due to the fact that stronger stochastic effects associated with small population levels in the initial phase of cell dynamics create the potential for population extinction to occur in some simulations of the IB model – *i.e.* under the exact same parameter setting, we can observe extinction or survival of the population in the IB model due to demographic stochasticity (cf. the single simulation results displayed in Figures 7 and 8). On the other hand, the cell population will always persist according to the PDE model. This ultimately results in discrepancies between the average behaviour of the IB model and the behaviour of the PDE model (cf. the plots in the bottom-line panels of Figures 5 and 6).

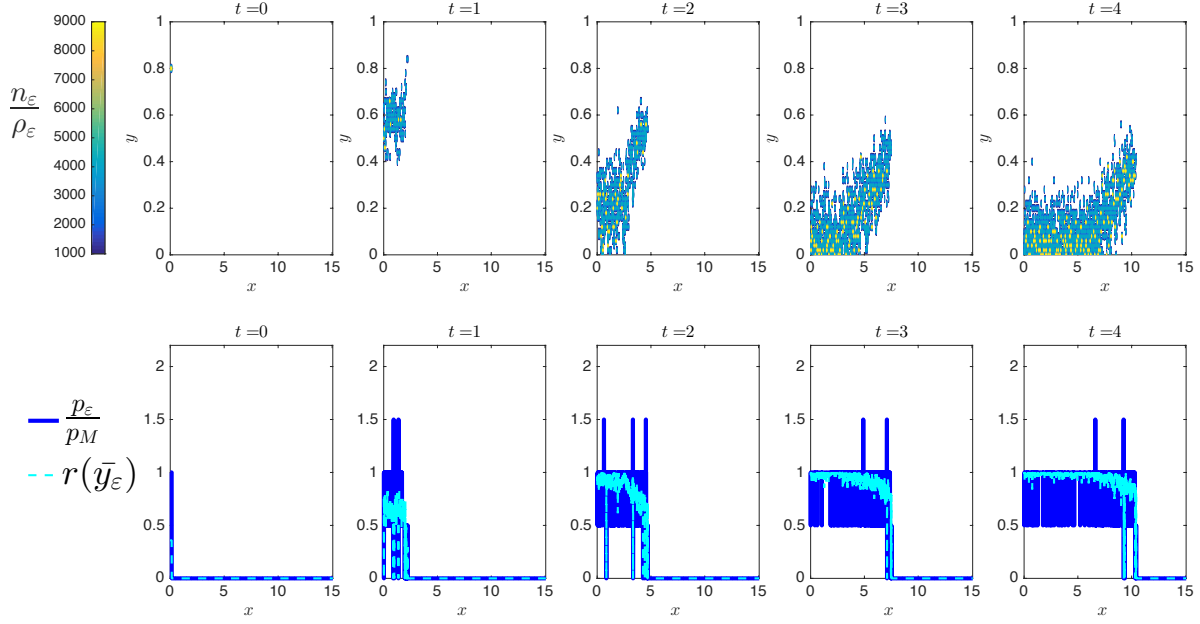


Figure 7: Numerical results of a single simulation of the IB model with $A_0 = 0.27$ and $\bar{y}^0 = 0.8$ in the initial cell distribution (4.8) – *i.e.* 1 out of the 10 simulations that are used to produce the average results displayed in the right-column, bottom-line panel of Figure 5. Plots display the scaled cell population density $n_\varepsilon/\rho_\varepsilon$ (top panels) and the scaled cell pressure p_ε/p_M (bottom panels, solid blue lines) at five successive time instants (*i.e.* $t = 0, t = 1, t = 2, t = 3$ and $t = 4$). The dashed cyan lines in the bottom panels highlight the corresponding values of $r(\bar{y}_\varepsilon)$, with \bar{y}_ε defined via (4.11). In this simulation, the cell population does not go extinct.

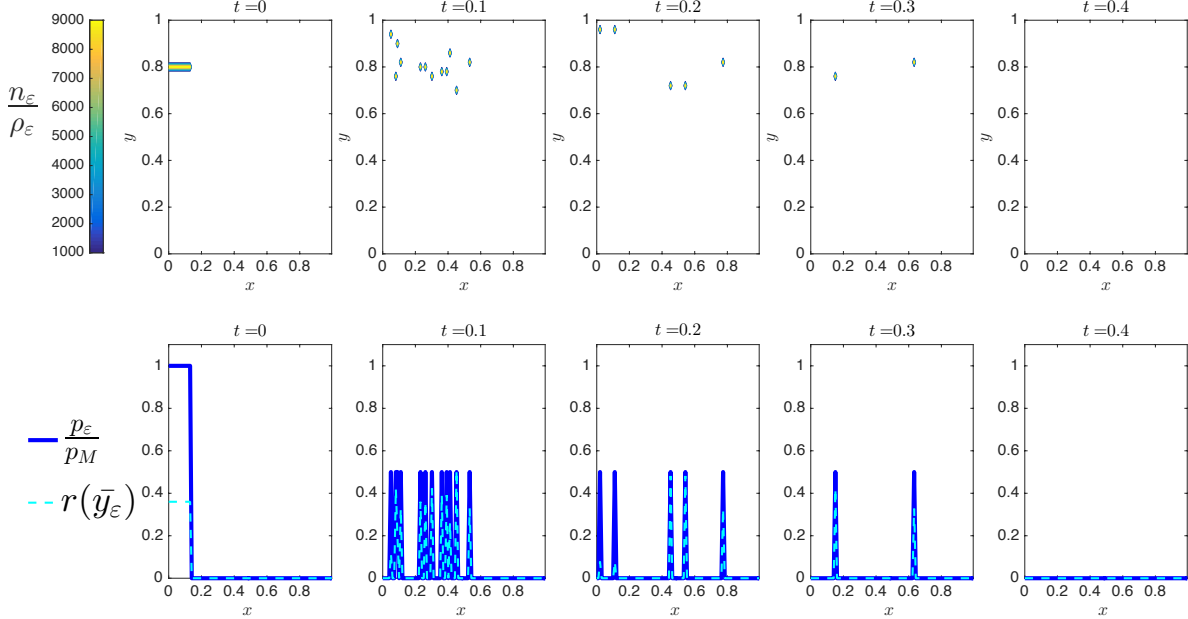


Figure 8: Numerical results of a single simulation of the IB model with $A_0 = 0.27$ and $\bar{y}^0 = 0.8$ in the initial cell distribution (4.8) – *i.e.* 1 out of the 10 simulations that are used to produce the average results displayed in the right-column, bottom-line panel of Figure 5. Plots display the scaled cell population density $n_\varepsilon/\rho_\varepsilon$ (top panels) and the scaled cell pressure p_ε/p_M (bottom panels, solid blue lines) at five successive time instants (*i.e.* $t = 0, t = 0.1, t = 0.2, t = 0.3$ and $t = 0.4$). The dashed cyan lines in the bottom panels highlight the corresponding values of $r(\bar{y}_\varepsilon)$, with \bar{y}_ε defined via (4.11). In this simulation, the cell population goes extinct rapidly.

5 Conclusions and research perspectives

We developed an IB model for the dynamics of phenotypically heterogeneous growing cell populations, which captures intercellular variability in cell proliferation and migration rates. We concentrated on a proliferation-migration tradeoff scenario, where the cell phenotypes span a spectrum of states from minimally-mobile but highly-proliferative to highly-mobile but minimally-proliferative. In the context of cancer invasion, such a tradeoff is the tenet of the “go-or-grow” hypothesis, which was conceived following observations of glioma cell behaviour [38] and has stimulated much empirical and theoretical research – see, for instance, [23, 33, 38, 42, 43, 74, 83, 86, 90] and references therein.

We reported on the results of numerical simulations of the IB model which illustrate how proliferation-migration tradeoffs shaping the evolutionary dynamics of single cells can lead, at the population level, to the generation of travelling waves whereby phenotypes are structured across the support of the wave, with highly-mobile cells being found at the invasive front and more-proliferative cells dominating at the rear. Similar patterns of cell population growth have been observed in gliomas, where cells within the interior of the tumour exhibit higher proliferation and lower migration rates, while cells on the tumour border are instead characterised by lower proliferation and higher migration rates [26, 37, 38, 87, 88].

We formally derived the deterministic continuum counterpart of the IB model, which comprises a non-local PDE for the cell population density function, and carried out a comparative study between numerical simulations of the IB model and both numerical solutions and formal travelling-wave analysis of the PDE model. We demonstrated that there is an excellent quantitative agreement between the results of numerical simulations of the IB model and the results of numerical simulations and travelling-wave analysis of the corresponding PDE model, when sufficiently large cell numbers are considered. This testifies to the robustness of the results of numerical simulations of the IB model presented here (see Remark 4).

In general, agreement between IB models and their continuum counterparts arises in regions of the model parameter space that correspond to sufficiently large cell numbers [64, 78, 80], while discrepancies may arise when the number of cells becomes low – *e.g.* if the rate of cell death is sufficiently large [52] – leading to possible extinction of the population in the IB model. We have provided numerical evidence of situations such as these in which the predictions of the two models can differ due to demographic stochasticity, which cannot be captured by the PDE model. This indicates the importance of integrating individual-based and continuum approaches when modelling the growth of phenotypically heterogeneous cell populations.

Although in this work we focused on a one-dimensional spatial domain scenario, the IB model presented here, and the formal limiting procedure to derive the corresponding continuum model, could easily be adapted to higher spatial dimensions. Furthermore, while we represented the spatial domain of the IB model as a regular lattice, it would certainly be interesting to generalise the underlying modelling approach, as well as the formal method to derive the continuum counterpart of the model, to cases where cells are distributed over irregular lattices and also to cases where off-lattice representations of the spatial domain are adopted. The present IB model could also be extended further to include the effects of chemical species (*e.g.* nutrients, growth factors, chemoattractants, chemorepulsants) and how the cells interact with and respond to these chemicals. To include and implement chemical species in the current model, we could use a hybrid modelling approach whereby the probabilistic rules governing the dynamics of single cells would be coupled with balance equations for the chemical concentrations. Hybrid modelling approaches of this type have been utilised in the context of modelling various aspects of cancer growth and development – see, for instance, [13, 47, 48, 60, 75, 77].

The generality of our assumptions makes the IB modelling framework presented here applicable to a broad range of biological processes that are driven by the growth of phenotypically heterogeneous cell populations, including tumour invasion and tissue remodelling and repair. It would thus be interesting to focus on particular cellular systems, and consequently define specific models, which could then be more accurately parameterised using precise biological data. This would offer the opportunity to dissect out the role played by different spatiotemporal evolutionary processes at the single-cell level in the formation of complex spatial patterns of population growth.

Acknowledgments

T.L. gratefully acknowledges support from the MIUR grant “Dipartimenti di Eccellenza 2018-2022” (Project no. E11G18000350001). F.R.M. gratefully acknowledges support from the RSE Saltire Early Career Fellowship ‘Multi-scale mathematical modelling of spatial eco-evolutionary cancer dynamics’ (Fellowship No. 1879).

Conflict of interest

The authors declare no competing interests.

References

- [1] C. A. Aktipis, A. M. Boddy, R. A. Gatenby, J. S. Brown, and C. C. Maley. Life history trade-offs in cancer evolution. *Nat. Rev. Cancer*, 13(12):883, 2013.
- [2] J. C. L. Alfonso, K. Talkenberger, M. Seifert, B. Klink, A. Hawkins-Daarud, K. R. Swanson, H. Hatzikirou, and A. Deutsch. The biology and mathematical modelling of glioma invasion: A review. *J. R. Soc. Interface*, 14(136):20170490, 2017.
- [3] D. Ambrosi and L. Preziosi. On the closure of mass balance models for tumor growth. *Math. Mod. Meth. Appl. Sci.*, 12(05):737–754, 2002.
- [4] A. R. A. Anderson, M. A. J. Chaplain, and K. Rejniak. *Single-cell-based models in biology and medicine*. Springer Science & Business Media, 2007.
- [5] A. Ardaševa, A. R. A. Anderson, R. A. Gatenby, H. M. Byrne, P. K. Maini, and T. Lorenzi. Comparative study between discrete and continuum models for the evolution of competing phenotype-structured cell populations in dynamical environments. *Phys. Rev. E*, 102(4):042404, 2020.
- [6] R. E. Baker, A. Parker, and M. J. Simpson. A free boundary model of epithelial dynamics. *J. Theor. Biol.*, 481:61–74, 2019.
- [7] G. Barles, L. C. Evans, and P. E. Souganidis. Wavefront propagation for reaction-diffusion systems of PDE. *Duke Math. J.*, 61(3):835–858, 1989.
- [8] G. Barles, S. Mirrahimi, and B. Perthame. Concentration in Lotka-Volterra parabolic or integral equations: A general convergence result. *Methods and Applications of Analysis*, 16(3):321–340, 2009.
- [9] M. Basan, T. Risler, J.F. Joanny, X. Sastre-Garau, and J. Prost. Homeostatic competition drives tumor growth and metastasis nucleation. *HFSP Journal*, 3(4):265–272, 2009.
- [10] D. Bresch, T. Colin, E. Grenier, B. Ribba, and O. Saut. Computational modeling of solid tumor growth: The avascular stage. *SIAM J. Sci. Comput.*, 32(4):2321–2344, 2010.
- [11] A. Brock, H. Chang, and S. Huang. Non-genetic heterogeneity—A mutation-independent driving force for the somatic evolution of tumours. *Nat. Rev. Genet.*, 10(5):336–342, 2009.
- [12] A. Brú, S. Albertos, J. L. Subiza, J. L. García-Asenjo, and I. Brú. The universal dynamics of tumor growth. *Biophys. J.*, 85(5):2948–2961, 2003.
- [13] F. Bubba, T. Lorenzi, and F. R. Macfarlane. From a discrete model of chemotaxis with volume-filling to a generalized Patlak-Keller-Segel model. *Proc. R. Soc. A*, 476(2237):20190871, 2020.
- [14] F. Bubba, B. Perthame, C. Pouchol, and M. Schmidtchen. Hele–shaw limit for a system of two reaction-(cross-) diffusion equations for living tissues. *Arch. Ration. Mech. Anal.*, 236(2):735–766, 2020.
- [15] H. M. Byrne and M. A. J. Chaplain. Free boundary value problems associated with the growth and development of multicellular spheroids. *Eur. J. Appl. Math.*, 8(6):639–658, 1997.
- [16] H. M. Byrne and D. Drasdo. Individual-based and continuum models of growing cell populations: A comparison. *J. Math. Biol.*, 58(4-5):657, 2009.
- [17] H. M. Byrne and L. Preziosi. Modelling solid tumour growth using the theory of mixtures. *Math. Med. Biol.*, 20(4):341–366, 2003.

- [18] M. A. J. Chaplain, C. Givero, T. Lorenzi, and L. Preziosi. Derivation and application of effective interface conditions for continuum mechanical models of cell invasion through thin membranes. *SIAM J. Appl. Math.*, 79(5):2011–2031, 2019.
- [19] M. A. J. Chaplain, T. Lorenzi, and F.R. Macfarlane. Bridging the gap between individual-based and continuum models of growing cell populations. *J. Math. Biol.*, 80(1):343–371, 2020.
- [20] R. H. Chisholm, T. Lorenzi, and J. Clairambault. Cell population heterogeneity and evolution towards drug resistance in cancer: Biological and mathematical assessment, theoretical treatment optimisation. *Biochim. Biophys. Acta, Gen. Subj.*, 1860(11):2627–2645, 2016.
- [21] R. H. Chisholm, T. Lorenzi, L. Desvillettes, and B. D. Hughes. Evolutionary dynamics of phenotype-structured populations: From individual-level mechanisms to population-level consequences. *Z. Angew. Math. Phys.*, 67(4):1–34, 2016.
- [22] P. Ciarletta, L. Foret, and M. Ben Amar. The radial growth phase of malignant melanoma: Multi-phase modelling, numerical simulations and linear stability analysis. *J. R. Soc. Interface*, 8(56):345–368, 2011.
- [23] A. Corcoran and R. F. Del Maestro. Testing the “go or grow” hypothesis in human medulloblastoma cell lines in two and three dimensions. *Neurosurgery*, 53(1):174–185, 2003.
- [24] N. David and X. Ruan. An asymptotic preserving scheme for a tumor growth model of porous medium type. *ESAIM Math. Model. Numer. Anal.*, 56(1):121–150, 2022.
- [25] C. Deroulers, M. Aubert, M. Badoual, and B. Grammaticos. Modeling tumor cell migration: From microscopic to macroscopic models. *Phys. Rev. E*, 79(3):031917, 2009.
- [26] H. D. Dhruv, W. S. McDonough Winslow, B. Armstrong, S. Tuncali, J. Eschbacher, K. Kislin, J. C. Loftus, N. L. Tran, and M. E. Berens. Reciprocal activation of transcription factors underlies the dichotomy between proliferation and invasion of glioma cells. *PLoS One*, 8(8), 2013.
- [27] O. Diekmann, P. E. Jabin, S. Mischler, and B. Perthame. The dynamics of adaptation: An illuminating example and a Hamilton–Jacobi approach. *Theor. Popul. Biol.*, 67(4):257–271, 2005.
- [28] D. Drasdo. Coarse graining in simulated cell populations. *Adv. Complex Syst.*, 8(02n03):319–363, 2005.
- [29] D. Drasdo and S. Hoehme. Modeling the impact of granular embedding media, and pulling versus pushing cells on growing cell clones. *New J. Phys.*, 14(5):055025, 2012.
- [30] L. Dyson, P. K. Maini, and R. E. Baker. Macroscopic limits of individual-based models for motile cell populations with volume exclusion. *Phys. Rev. E*, 86(3):031903, 2012.
- [31] L. C. Evans and P. E. Souganidis. A PDE approach to geometric optics for certain semilinear parabolic equations. *Indiana Univ. Math. J.*, 38(1):141–172, 1989.
- [32] W. H. Fleming and P. E. Souganidis. PDE-viscosity solution approach to some problems of large deviations. *Ann. Sc. Norm. Super. Pisa - Cl. sci.*, 13(2):171–192, 1986.
- [33] J. A. Gallaher, J. S. Brown, and A. R. A. Anderson. The impact of proliferation-migration tradeoffs on phenotypic evolution in cancer. *Sci. Rep.*, 9(1):1–10, 2019.
- [34] O. Gallinato, T. Colin, O. Saut, and C. Poinard. Tumor growth model of ductal carcinoma: From in situ phase to stroma invasion. *J. Theor. Biol.*, 429:253–266, 2017.
- [35] P. Gerlee and A. R. A. Anderson. Evolution of cell motility in an individual-based model of tumour growth. *J. Theor. Biol.*, 259(1):67–83, 2009.
- [36] P. Gerlee and S. Nelander. The impact of phenotypic switching on glioblastoma growth and invasion. *PLoS Comput. Biol.*, 8(6):e1002556, 2012.

- [37] A. Giese, R. Bjerkvig, M. E. Berens, and M. Westphal. Cost of migration: invasion of malignant gliomas and implications for treatment. *J. Clin. Oncol.*, 21(8):1624–1636, 2003.
- [38] A. Giese, M. A. Loo, N. Tran, D. Haskett, S. W. Coons, and M. E. Berens. Dichotomy of astrocytoma migration and proliferation. *Int. J. Cancer.*, 67(2):275–282, 1996.
- [39] C. Giverso and P. Ciarletta. On the morphological stability of multicellular tumour spheroids growing in porous media. *Eur. Phys. J. E*, 39(10), 2016.
- [40] J. Godlewski, A. Bronisz, M. O. Nowicki, E. A. Chiocca, and S. Lawler. microRNA-451: A conditional switch controlling glioma cell proliferation and migration. *Cell Cycle*, 9(14):2814–2820, 2010.
- [41] H. P. Greenspan. On the growth and stability of cell cultures and solid tumors. *J. Theor. Biol.*, 56(1):229–242, 1976.
- [42] H. Hatzikirou, D. Basanta, M. Simon, K. Schaller, and A. Deutsch. ‘go or grow’: the key to the emergence of invasion in tumour progression? *Math. Med. Biol.*, 29(1):49–65, 2012.
- [43] K. S. Hoek, O. M. Eichhoff, N. C. Schlegel, U. Döbbeling, N. Kobert, L. Schaerer, S. Hemmi, and R. Dummer. In vivo switching of human melanoma cells between proliferative and invasive states. *Cancer Res.*, 68(3):650–656, 2008.
- [44] S. Huang. Genetic and non-genetic instability in tumor progression: Link between the fitness landscape and the epigenetic landscape of cancer cells. *Cancer Metastasis Rev.*, 32(3):423–448, 2013.
- [45] B. D. Hughes. *Random walks and random environments: random walks*, volume 1. Oxford University Press, 1995.
- [46] M. Inoue. Derivation of a porous medium equation from many markovian particles and the propagation of chaos. *Hiroshima Math. J.*, 21(1):85–110, 1991.
- [47] S. Jafari Nivlouei, M. Soltani, J. Carvalho, R. Travasso, M. R. Salimpour, and E. Shirani. Multiscale modeling of tumor growth and angiogenesis: Evaluation of tumor-targeted therapy. *PLoS Comp. Biol.*, 17(6):e1009081, 2021.
- [48] S. Jafari Nivlouei, M. Soltani, E. Shirani, M. R. Salimpour, R. Travasso, and J. Carvalho. A multiscale cell-based model of tumor growth for chemotherapy assessment and tumor-targeted therapy through a 3D computational approach. *Cell Prolif.*, page e13187, 2022.
- [49] S. T. Johnston, R. E. Baker, D. L. McElwain, and M. J. Simpson. Co-operation, competition and crowding: A discrete framework linking allee kinetics, nonlinear diffusion, shocks and sharp-fronted travelling waves. *Sci. Rep.*, 7(1):1–19, 2017.
- [50] S. T. Johnston, M. J. Simpson, and R. E. Baker. Mean-field descriptions of collective migration with strong adhesion. *Phys. Rev. E*, 85(5):051922, 2012.
- [51] S. T. Johnston, M. J. Simpson, and R. E. Baker. Modelling the movement of interacting cell populations: A moment dynamics approach. *J. Theor. Biol.*, 370:81–92, 2015.
- [52] S.T. Johnston, M. J. Simpson, and E. J. Crampin. Predicting population extinction in lattice-based birth–death–movement models. *Proc. Roy. Soc. A*, 476(2238):20200089, 2020.
- [53] M. Kuznetsov, J. Clairambault, and V. Volpert. Improving cancer treatments via dynamical biophysical models. *Phys. Life Rev.*, 39:1–48, 2021.
- [54] T. Lorenzi. Cancer modelling as fertile ground for new mathematical challenges. *Phys. Life Rev.*, 40:3–5, 2022.
- [55] T. Lorenzi, A. Lorz, and B. Perthame. On interfaces between cell populations with different mobilities. *Kinet. Relat. Mod.*, 10(1):299–311, 2017.

- [56] T. Lorenzi, P. J. Murray, and M. Ptashnyk. From individual-based mechanical models of multicellular systems to free-boundary problems. *Interface Free Bound.*, 22(2):205–244, 2020.
- [57] T. Lorenzi and K. J. Painter. Trade-offs between chemotaxis and proliferation shape the phenotypic structuring of invading waves. *Int. J. Non Linear Mech.*, 139:103885, 2022.
- [58] T. Lorenzi, B. Perthame, and X. Ruan. Invasion fronts and adaptive dynamics in a model for the growth of cell populations with heterogeneous mobility. *Eur. J. Appl. Math.*, pages 1–18, 2021.
- [59] A. Lorz, S. Mirrahimi, and B. Perthame. Dirac mass dynamics in multidimensional nonlocal parabolic equations. *Commun. Partial. Differ. Equ.*, 36(6):1071–1098, 2011.
- [60] J. S. Lowengrub, H. B. Frieboes, F. Jin, Y.L. Chuang, X. Li, P. Macklin, S. M. Wise, and V. Cristini. Nonlinear modelling of cancer: Bridging the gap between cells and tumours. *Nonlinearity*, 23(1):R1, 2009.
- [61] F. R. Macfarlane, M. A. J. Chaplain, and T. Lorenzi. A hybrid discrete-continuum approach to model Turing pattern formation. *Math. Biosci. Eng.*, 17(6):7442–7479, 2020.
- [62] P. J. Murray, C. M. Edwards, M. J. Tindall, and P. K. Maini. From a discrete to a continuum model of cell dynamics in one dimension. *Phys. Rev. E*, 80(3):031912, 2009.
- [63] P. J. Murray, C. M. Edwards, M. J. Tindall, and P. K. Maini. Classifying general nonlinear force laws in cell-based models via the continuum limit. *Phys. Rev. E*, 85(2):021921, 2012.
- [64] J. T. Nardini, R. E. Baker, M. J. Simpson, and K. B. Flores. Learning differential equation models from stochastic agent-based model simulations. *J. Roy. Soc. Interface*, 18(176):20200987, 2021.
- [65] N. M. Novikov, S. Y. Zolotaryova, A. M. Gautreau, and E. V. Denisov. Mutational drivers of cancer cell migration and invasion. *Br. J. Cancer*, 124(1):102–114, 2021.
- [66] K. Oelschläger. On the derivation of reaction-diffusion equations as limit dynamics of systems of moderately interacting stochastic processes. *Probab. Theory Relat. Fields*, 82(4):565–586, 1989.
- [67] K. Oelschläger. Large systems of interacting particles and the porous medium equation. *J. Differ. Equ.*, 88(2):294–346, 1990.
- [68] P. A. Orlando, R. A. Gatenby, and J. S. Brown. Tumor evolution in space: The effects of competition colonization tradeoffs on tumor invasion dynamics. *Front. Oncol.*, 3:45, 2013.
- [69] C. J. Penington, B. D. Hughes, and K. A. Landman. Building macroscale models from microscale probabilistic models: A general probabilistic approach for nonlinear diffusion and multispecies phenomena. *Phys. Rev. E*, 84(4):041120, 2011.
- [70] B. Perthame. *Transport equations in biology*. Springer Science & Business Media, 2006.
- [71] B. Perthame. Some mathematical aspects of tumor growth and therapy. In *ICM 2014-International Congress of Mathematicians*, 2014.
- [72] B. Perthame and G. Barles. Dirac concentrations in Lotka-Volterra parabolic PDEs. *Indiana Univ. Math. J.*, 57(7):3275–3301, 2008.
- [73] B. Perthame, F. Quirós, and J. L. Vázquez. The Hele-Shaw asymptotics for mechanical models of tumor growth. *Arch. Ration. Mech. Anal.*, 212(1):93–127, 2014.
- [74] K. Pham, A. Chauviere, H. Hatzikirou, X. Li, H. M. Byrne, V. Cristini, and J. Lowengrub. Density-dependent quiescence in glioma invasion: Instability in a simple reaction–diffusion model for the migration/proliferation dichotomy. *J. Biol. Dyn.*, 6(sup1):54–71, 2012.
- [75] G. G. Powathil, M. Swat, and M. A. J. Chaplain. Systems oncology: towards patient-specific treatment regimes informed by multiscale mathematical modelling. In *Sem. Cancer Biol.*, volume 30, pages 13–20. Elsevier, 2015.

- [76] J. Ranft, M. Basan, J. Elgeti, J.F. Joanny, J. Prost, and F. Jülicher. Fluidization of tissues by cell division and apoptosis. *Proc. Nat. Acad. Sci. USA*, 107(49):20863–20868, 2010.
- [77] K. A. Rejniak and A. R. A. Anderson. Hybrid models of tumor growth. *Wiley Interdiscip. Rev. Syst. Biol. Med.*, 3(1):115–125, 2011.
- [78] M. J. Simpson, R. E. Baker, P. R. Buenzli, R. Nicholson, and O. J. Maclaren. Reliable and efficient parameter estimation using approximate continuum limit descriptions of stochastic models. *bioRxiv*, 2022.
- [79] M. J. Simpson, A. Merrifield, K. A. Landman, and B. D. Hughes. Simulating invasion with cellular automata: Connecting cell-scale and population-scale properties. *Phys. Rev. E*, 76(2):021918, 2007.
- [80] M. J. Simpson, J. A. Sharp, and R. E. Baker. Distinguishing between mean-field, moment dynamics and stochastic descriptions of birth–death–movement processes. *Phys. A: Stat. Mech. Appl.*, 395:236–246, 2014.
- [81] J. T. Smith, J. K. Tomfohr, M. C. Wells, T. P. Beebe, T. B. Kepler, and W. M. Reichert. Measurement of cell migration on surface-bound fibronectin gradients. *Langmuir*, 20(19):8279–8286, 2004.
- [82] R. E. A. Stace, T. Stiehl, M. A. J. Chaplain, A. Marciniak-Czochra, and T. Lorenzi. Discrete and continuum phenotype-structured models for the evolution of cancer cell populations under chemotherapy. *Math. Mod. Nat. Phen.*, 15:14, 2020.
- [83] T. L. Stepien, E. M. Rutter, and Y. Kuang. Traveling waves of a go-or-grow model of glioma growth. *SIAM J. Appl. Math.*, 78(3):1778–1801, 2018.
- [84] M. Tang, N. Vauchelet, I. Cheddadi, I. Vignon-Clementel, D. Drasdo, and B. Perthame. Composite waves for a cell population system modeling tumor growth and invasion. *Chinese Ann. Math. Ser. B*, 34(2):295–318, 2013.
- [85] P. Van Liedekerke, M. M. Palm, N. Jagiella, and D. Drasdo. Simulating tissue mechanics with agent-based models: Concepts, perspectives and some novel results. *Comput. Part. Mech.*, 2(4):401–444, 2015.
- [86] S. T. Vittadello, S. W. McCue, G. Gunasingh, N. K. Haass, and M. J. Simpson. Examining go-or-grow using fluorescent cell-cycle indicators and cell-cycle-inhibiting drugs. *Biophys. J.*, 118(6):1243–1247, 2020.
- [87] S. D. Wang, P. Rath, B. Lal, J. P. Richard, Y. Li, C. R. Goodwin, J. Laterra, and S. Xia. EphB2 receptor controls proliferation/migration dichotomy of glioblastoma by interacting with focal adhesion kinase. *Oncogene*, 31(50):5132–5143, 2012.
- [88] Q. Xie, S. Mittal, and M. E. Berens. Targeting adaptive glioblastoma: An overview of proliferation and invasion. *Neuro-Oncol.*, 16(12):1575–1584, 2014.
- [89] M. Yan, X. Yang, R. Shen, C. Wu, H. Wang, Q. Ye, P. Yang, L. Zhang, M. Chen, B. Wan, et al. miR-146b promotes cell proliferation and increases chemosensitivity, but attenuates cell migration and invasion via FBXL10 in ovarian cancer. *Cell Death Dis.*, 9(11):1–17, 2018.
- [90] A. Zhigun, C. Surulescu, and A. Hunt. A strongly degenerate diffusion-haptotaxis model of tumour invasion under the go-or-grow dichotomy hypothesis. *Math. Methods Appl. Sci.*, 41(6):2403–2428, 2018.

Appendices

A Formal derivation of the continuum model

Building on the methods that we previously employed in [5, 13, 19, 61, 82], here we show that the non-local PDE (3.2) can be formally derived as the appropriate continuum limit of the IB model developed in this paper.

In the case where, between time-steps k and $k + 1$, each cell in phenotypic state $y_j \in (0, Y)$ at position $x_i \in \mathbb{R}$ can first move, next undergo phenotypic changes and then die or divide according to the rules described in Section 2, the principle of mass balance gives the following difference equation

$$\begin{aligned}
 n_{i,j}^{k+1} = & n_{i+1,j+1}^k \left\{ \frac{\lambda}{2} [1 + \tau R(y_j, p_i^k)] \frac{\nu\mu(y_j)}{2p_M} (p_{i+1}^k - p_i^k)_+ \right\} \\
 & + n_{i-1,j+1}^k \left\{ \frac{\lambda}{2} [1 + \tau R(y_j, p_i^k)] \frac{\nu\mu(y_j)}{2p_M} (p_{i-1}^k - p_i^k)_+ \right\} \\
 & + n_{i+1,j-1}^k \left\{ \frac{\lambda}{2} [1 + \tau R(y_j, p_i^k)] \frac{\nu\mu(y_j)}{2p_M} (p_{i+1}^k - p_i^k)_+ \right\} \\
 & + n_{i-1,j-1}^k \left\{ \frac{\lambda}{2} [1 + \tau R(y_j, p_i^k)] \frac{\nu\mu(y_j)}{2p_M} (p_{i-1}^k - p_i^k)_+ \right\} \\
 & + n_{i,j+1}^k \left\{ \frac{\lambda}{2} [1 + \tau R(y_j, p_i^k)] \left[1 - \frac{\nu\mu(y_j)}{2p_M} [(p_i^k - p_{i+1}^k)_+ + (p_i^k - p_{i-1}^k)_+] \right] \right\} \\
 & + n_{i,j-1}^k \left\{ \frac{\lambda}{2} [1 + \tau R(y_j, p_i^k)] \left[1 - \frac{\nu\mu(y_j)}{2p_M} [(p_i^k - p_{i+1}^k)_+ + (p_i^k - p_{i-1}^k)_+] \right] \right\} \\
 & + n_{i+1,j}^k \left\{ (1 - \lambda) [1 + \tau R(y_j, p_i^k)] \frac{\nu\mu(y_j)}{2p_M} (p_{i+1}^k - p_i^k)_+ \right\} \\
 & + n_{i-1,j}^k \left\{ (1 - \lambda) [1 + \tau R(y_j, p_i^k)] \frac{\nu\mu(y_j)}{2p_M} (p_{i-1}^k - p_i^k)_+ \right\} \\
 & + n_{i,j}^k \left\{ (1 - \lambda) [1 + \tau R(y_j, p_i^k)] \left[1 - \frac{\nu\mu(y_j)}{2p_M} [(p_i^k - p_{i+1}^k)_+ + (p_i^k - p_{i-1}^k)_+] \right] \right\}.
 \end{aligned} \tag{A.1}$$

Using the fact that for τ, χ and η sufficiently small the following relations hold

$$n_{i,j}^k \approx n(t, x, y), \quad n_{i,j}^{k+1} \approx n(t + \tau, x, y), \quad n_{i\pm 1,j}^k \approx n(t, x \pm \chi, y), \quad n_{i,j\pm 1}^k \approx n(t, x, y \pm \eta)$$

$$\rho_i^k \approx \rho(t, x) := \int_0^Y n(t, x, y) dy, \quad p_i^k \approx p(t, x) = \Pi[\rho](t, x), \quad p_{i\pm 1}^k \approx p(t, x \pm \chi) = \Pi[\rho](t, x \pm \chi),$$

equation (A.1) can be formally rewritten in the approximate form

$$\begin{aligned}
 n(t + \tau, x, y) = & n(t, x + \chi, y + \eta) \left\{ \frac{\lambda}{2} [1 + \tau R(y, p)] \frac{\nu\mu(y)}{2p_M} (p(t, x + \chi) - p)_+ \right\} \\
 & + n(t, x - \chi, y + \eta) \left\{ \frac{\lambda}{2} [1 + \tau R(y, p)] \frac{\nu\mu(y)}{2p_M} (p(t, x - \chi) - p)_+ \right\} \\
 & + n(t, x + \chi, y - \eta) \left\{ \frac{\lambda}{2} [1 + \tau R(y, p)] \frac{\nu\mu(y)}{2p_M} (p(t, x + \chi) - p)_+ \right\} \\
 & + n(t, x - \chi, y - \eta) \left\{ \frac{\lambda}{2} [1 + \tau R(y, p)] \frac{\nu\mu(y)}{2p_M} (p(t, x - \chi) - p)_+ \right\} \\
 & + n(t, x, y + \eta) \left\{ \frac{\lambda}{2} [1 + \tau R(y, p)] \left[1 - \frac{\nu\mu(y)}{2p_M} [(p - p(t, x + \chi))_+ + (p - p(t, x - \chi))_+] \right] \right\} \\
 & + n(t, x, y - \eta) \left\{ \frac{\lambda}{2} [1 + \tau R(y, p)] \left[1 - \frac{\nu\mu(y)}{2p_M} [(p - p(t, x + \chi))_+ + (p - p(t, x - \chi))_+] \right] \right\}
 \end{aligned} \tag{A.2}$$

$$\begin{aligned}
& +n(t, x + \chi, y) \left\{ (1 - \lambda) [1 + \tau R(y, p)] \frac{\nu\mu(y)}{2p_M} (p(t, x + \chi) - p)_+ \right\} \\
& +n(t, x - \chi, y) \left\{ (1 - \lambda) [1 + \tau R(y, p)] \frac{\nu\mu(y)}{2p_M} (p(t, x - \chi) - p)_+ \right\} \\
& +n \left\{ (1 - \lambda) [1 + \tau R(y, p)] \left[1 - \frac{\nu\mu(y)}{2p_M} (p - p(t, x + \chi))_+ - \frac{\nu\mu(y)}{2p_M} (p - p(t, x - \chi))_+ \right] \right\},
\end{aligned}$$

where $n \equiv n(t, x, y)$ and $p \equiv p(t, x)$. If the function $n(t, x, y)$ is twice continuously differentiable with respect to the variables y and x , for η and χ sufficiently small we can then use the Taylor expansions

$$n(t, x, y \pm \eta) = n \pm \eta \frac{\partial n}{\partial y} + \frac{\eta^2}{2} \frac{\partial^2 n}{\partial y^2} + \text{h.o.t.}, \quad n(t, x \pm \chi, y) = n \pm \chi \frac{\partial n}{\partial x} + \frac{\chi^2}{2} \frac{\partial^2 n}{\partial x^2} + \text{h.o.t.},$$

$$n(t, x + \chi, y \pm \eta) = n + \chi \frac{\partial n}{\partial x} \pm \eta \frac{\partial n}{\partial y} + \frac{\chi^2}{2} \frac{\partial^2 n}{\partial x^2} + \frac{\eta^2}{2} \frac{\partial^2 n}{\partial y^2} \pm \chi \eta \frac{\partial^2 n}{\partial x \partial y} + \text{h.o.t.}$$

and

$$n(t, x - \chi, y \pm \eta) = n - \chi \frac{\partial n}{\partial x} \pm \eta \frac{\partial n}{\partial y} + \frac{\chi^2}{2} \frac{\partial^2 n}{\partial x^2} + \frac{\eta^2}{2} \frac{\partial^2 n}{\partial y^2} \mp \chi \eta \frac{\partial^2 n}{\partial x \partial y} + \text{h.o.t.},$$

which allow us to rewrite equation (A.2) as

$$\begin{aligned}
n(t + \tau, x, y) = & n \left\{ \frac{\lambda}{2} [1 + \tau R(y, p)] \frac{\nu\mu(y)}{2p_M} (p(t, x + \chi) - p)_+ \right\} \\
& + \chi \frac{\partial n}{\partial x} \left\{ \frac{\lambda}{2} [1 + \tau R(y, p)] \frac{\nu\mu(y)}{2p_M} (p(t, x + \chi) - p)_+ \right\} \\
& + \eta \frac{\partial n}{\partial y} \left\{ \frac{\lambda}{2} [1 + \tau R(y, p)] \frac{\nu\mu(y)}{2p_M} (p(t, x + \chi) - p)_+ \right\} \\
& + \frac{\chi^2}{2} \frac{\partial^2 n}{\partial x^2} \left\{ \frac{\lambda}{2} [1 + \tau R(y, p)] \frac{\nu\mu(y)}{2p_M} (p(t, x + \chi) - p)_+ \right\} \\
& + \frac{\eta^2}{2} \frac{\partial^2 n}{\partial y^2} \left\{ \frac{\lambda}{2} [1 + \tau R(y, p)] \frac{\nu\mu(y)}{2p_M} (p(t, x + \chi) - p)_+ \right\} \\
& + \chi \eta \frac{\partial^2 n}{\partial x \partial y} \left\{ \frac{\lambda}{2} [1 + \tau R(y, p)] \frac{\nu\mu(y)}{2p_M} (p(t, x + \chi) - p)_+ \right\} \\
& + n \left\{ \frac{\lambda}{2} [1 + \tau R(y, p)] \frac{\nu\mu(y)}{2p_M} (p(t, x - \chi) - p)_+ \right\} \\
& - \chi \frac{\partial n}{\partial x} \left\{ \frac{\lambda}{2} [1 + \tau R(y, p)] \frac{\nu\mu(y)}{2p_M} (p(t, x - \chi) - p)_+ \right\} \\
& + \eta \frac{\partial n}{\partial y} \left\{ \frac{\lambda}{2} [1 + \tau R(y, p)] \frac{\nu\mu(y)}{2p_M} (p(t, x - \chi) - p)_+ \right\} \\
& + \frac{\chi^2}{2} \frac{\partial^2 n}{\partial x^2} \left\{ \frac{\lambda}{2} [1 + \tau R(y, p)] \frac{\nu\mu(y)}{2p_M} (p(t, x - \chi) - p)_+ \right\} \\
& + \frac{\eta^2}{2} \frac{\partial^2 n}{\partial y^2} \left\{ \frac{\lambda}{2} [1 + \tau R(y, p)] \frac{\nu\mu(y)}{2p_M} (p(t, x - \chi) - p)_+ \right\} \\
& - \chi \eta \frac{\partial^2 n}{\partial x \partial y} \left\{ \frac{\lambda}{2} [1 + \tau R(y, p)] \frac{\nu\mu(y)}{2p_M} (p(t, x - \chi) - p)_+ \right\} \\
& + n \left\{ \frac{\lambda}{2} [1 + \tau R(y, p)] \frac{\nu\mu(y)}{2p_M} (p(t, x + \chi) - p)_+ \right\} \\
& + \chi \frac{\partial n}{\partial x} \left\{ \frac{\lambda}{2} [1 + \tau R(y, p)] \frac{\nu\mu(y)}{2p_M} (p(t, x + \chi) - p)_+ \right\}
\end{aligned} \tag{A.3}$$

$$\begin{aligned}
& -\eta \frac{\partial n}{\partial y} \left\{ \frac{\lambda}{2} [1 + \tau R(y, p)] \frac{\nu \mu(y)}{2p_M} (p(t, x + \chi) - p)_+ \right\} \\
& + \frac{\chi^2}{2} \frac{\partial^2 n}{\partial x^2} \left\{ \frac{\lambda}{2} [1 + \tau R(y, p)] \frac{\nu \mu(y)}{2p_M} (p(t, x + \chi) - p)_+ \right\} \\
& + \frac{\eta^2}{2} \frac{\partial^2 n}{\partial y^2} \left\{ \frac{\lambda}{2} [1 + \tau R(y, p)] \frac{\nu \mu(y)}{2p_M} (p(t, x + \chi) - p)_+ \right\} \\
& - \chi \eta \frac{\partial^2 n}{\partial x \partial y} \left\{ \frac{\lambda}{2} [1 + \tau R(y, p)] \frac{\nu \mu(y)}{2p_M} (p(t, x + \chi) - p)_+ \right\} \\
& + n \left\{ \frac{\lambda}{2} [1 + \tau R(y, p)] \frac{\nu \mu(y)}{2p_M} (p(t, x - \chi) - p)_+ \right\} \\
& - \chi \frac{\partial n}{\partial x} \left\{ \frac{\lambda}{2} [1 + \tau R(y, p)] \frac{\nu \mu(y)}{2p_M} (p(t, x - \chi) - p)_+ \right\} \\
& - \eta \frac{\partial n}{\partial y} \left\{ \frac{\lambda}{2} [1 + \tau R(y, p)] \frac{\nu \mu(y)}{2p_M} (p(t, x - \chi) - p)_+ \right\} \\
& + \frac{\chi^2}{2} \frac{\partial^2 n}{\partial x^2} \left\{ \frac{\lambda}{2} [1 + \tau R(y, p)] \frac{\nu \mu(y)}{2p_M} (p(t, x - \chi) - p)_+ \right\} \\
& + \frac{\eta^2}{2} \frac{\partial^2 n}{\partial y^2} \left\{ \frac{\lambda}{2} [1 + \tau R(y, p)] \frac{\nu \mu(y)}{2p_M} (p(t, x - \chi) - p)_+ \right\} \\
& + \chi \eta \frac{\partial^2 n}{\partial x \partial y} \left\{ \frac{\lambda}{2} [1 + \tau R(y, p)] \frac{\nu \mu(y)}{2p_M} (p(t, x - \chi) - p)_+ \right\} \\
& + n \left\{ \frac{\lambda}{2} [1 + \tau R(y, p)] \left[1 - \frac{\nu \mu(y)}{2p_M} [(p - p(t, x + \chi))_+ + (p - p(t, x - \chi))_+] \right] \right\} \\
& + \eta \frac{\partial n}{\partial y} \left\{ \frac{\lambda}{2} [1 + \tau R(y, p)] \left[1 - \frac{\nu \mu(y)}{2p_M} [(p - p(t, x + \chi))_+ + (p - p(t, x - \chi))_+] \right] \right\} \\
& + \frac{\eta^2}{2} \frac{\partial^2 n}{\partial y^2} \left\{ \frac{\lambda}{2} [1 + \tau R(y, p)] \left[1 - \frac{\nu \mu(y)}{2p_M} [(p - p(t, x + \chi))_+ + (p - p(t, x - \chi))_+] \right] \right\} \\
& + n \left\{ \frac{\lambda}{2} [1 + \tau R(y, p)] \left[1 - \frac{\nu \mu(y)}{2p_M} [(p - p(t, x + \chi))_+ + (p - p(t, x - \chi))_+] \right] \right\} \\
& - \eta \frac{\partial n}{\partial y} \left\{ \frac{\lambda}{2} [1 + \tau R(y, p)] \left[1 - \frac{\nu \mu(y)}{2p_M} [(p - p(t, x + \chi))_+ + (p - p(t, x - \chi))_+] \right] \right\} \\
& + \frac{\eta^2}{2} \frac{\partial^2 n}{\partial y^2} \left\{ \frac{\lambda}{2} [1 + \tau R(y, p)] \left[1 - \frac{\nu \mu(y)}{2p_M} [(p - p(t, x + \chi))_+ + (p - p(t, x - \chi))_+] \right] \right\} \\
& + n \left\{ (1 - \lambda) [1 + \tau R(y, p)] \frac{\nu \mu(y)}{2p_M} (p(t, x + \chi) - p)_+ \right\} \\
& + \chi \frac{\partial n}{\partial x} \left\{ (1 - \lambda) [1 + \tau R(y, p)] \frac{\nu \mu(y)}{2p_M} (p(t, x + \chi) - p)_+ \right\} \\
& + \frac{\chi^2}{2} \frac{\partial^2 n}{\partial x^2} \left\{ (1 - \lambda) [1 + \tau R(y, p)] \frac{\nu \mu(y)}{2p_M} (p(t, x + \chi) - p)_+ \right\} \\
& + n \left\{ (1 - \lambda) [1 + \tau R(y, p)] \frac{\nu \mu(y)}{2p_M} (p(t, x - \chi) - p)_+ \right\} \\
& - \chi \frac{\partial n}{\partial x} \left\{ (1 - \lambda) [1 + \tau R(y, p)] \frac{\nu \mu(y)}{2p_M} (p(t, x - \chi) - p)_+ \right\} \\
& + \frac{\chi^2}{2} \frac{\partial^2 n}{\partial x^2} \left\{ (1 - \lambda) [1 + \tau R(y, p)] \frac{\nu \mu(y)}{2p_M} (p(t, x - \chi) - p)_+ \right\} \\
& + n \left\{ (1 - \lambda) [1 + \tau R(y, p)] \left[1 - \frac{\nu \mu(y)}{2p_M} (p - p(t, x + \chi))_+ - \frac{\nu \mu(y)}{2p_M} (p - p(t, x - \chi))_+ \right] \right\} + \text{h.o.t.}
\end{aligned}$$

Collecting terms that contain the same derivative of n we can further simplify equation (A.3) to obtain

$$\begin{aligned}
n(t + \tau, x, y) &= n[1 + \tau R(y, p)] \\
&+ n \left\{ [1 + \tau R(y, p)] \frac{\nu\mu(y)}{2p_M} [(p(t, x + \chi) - p)_+ + (p(t, x - \chi) - p)_+] \right\} \\
&- n \left\{ [1 + \tau R(y, p)] \frac{\nu\mu(y)}{2p_M} [(p - p(t, x + \chi))_+ + (p - p(t, x - \chi))_+] \right\} \\
&+ \chi \frac{\partial n}{\partial x} \left\{ [1 + \tau R(y, p)] \frac{\nu\mu(y)}{2p_M} [(p(t, x + \chi) - p)_+ - (p(t, x - \chi) - p)_+] \right\} \\
&+ \frac{\chi^2}{2} \frac{\partial^2 n}{\partial x^2} \left\{ [1 + \tau R(y, p)] \frac{\nu\mu(y)}{2p_M} [(p(t, x + \chi) - p)_+ + (p(t, x - \chi) - p)_+] \right\} \\
&+ \frac{\eta^2}{2} \frac{\partial^2 n}{\partial y^2} \left\{ \lambda [1 + \tau R(y, p)] \frac{\nu\mu(y)}{2p_M} [(p(t, x + \chi) - p)_+ + (p(t, x - \chi) - p)_+] \right\} \\
&- \frac{\eta^2}{2} \frac{\partial^2 n}{\partial y^2} \left\{ \lambda [1 + \tau R(y, p)] \frac{\nu\mu(y)}{2p_M} [(p - p(t, x + \chi))_+ + (p - p(t, x - \chi))_+] \right\} \\
&+ \frac{\lambda \eta^2}{2} \frac{\partial^2 n}{\partial y^2} [1 + \tau R(y, p)] + \text{h.o.t.} .
\end{aligned} \tag{A.4}$$

Rewriting the above equation by using the fact that

$$\begin{aligned}
&[(p(t, x + \chi) - p)_+ + (p(t, x - \chi) - p)_+] \\
&- [(p - p(t, x + \chi))_+ + (p - p(t, x - \chi))_+] = p(t, x + \chi) + p(t, x - \chi) - 2p,
\end{aligned}$$

dividing both sides of the resulting equation by τ , rearranging terms and then multiplying and dividing the terms on the right-hand side by either χ^2 or χ we find

$$\begin{aligned}
\frac{n(t + \tau, x, y) - n}{\tau} &= R(y, p) n + \frac{\lambda \eta^2}{2\tau} \frac{\partial^2 n}{\partial y^2} [1 + \tau R(y, p)] \\
&+ \frac{\nu \chi^2}{2\tau} n \left\{ [1 + \tau R(y, p)] \frac{\mu(y)}{p_M} \left[\frac{p(t, x + \chi) + p(t, x - \chi) - 2p}{\chi^2} \right] \right\} \\
&+ \frac{\nu \chi^2}{2\tau} \frac{\partial n}{\partial x} \left\{ [1 + \tau R(y, p)] \frac{\mu(y)}{p_M} \left[\left(\frac{p(t, x + \chi) - p}{\chi} \right)_+ - \left(\frac{p(t, x - \chi) - p}{\chi} \right)_+ \right] \right\} \\
&+ \frac{\chi}{2} \frac{\nu \chi^2}{2\tau} \frac{\partial^2 n}{\partial x^2} \left\{ [1 + \tau R(y, p)] \frac{\mu(y)}{p_M} \left[\left(\frac{p(t, x + \chi) - p}{\chi} \right)_+ + \left(\frac{p(t, x - \chi) - p}{\chi} \right)_+ \right] \right\} \\
&+ \frac{\eta^2}{2} \frac{\nu \chi^2}{2\tau} \frac{\partial^2 n}{\partial y^2} \left\{ \lambda [1 + \tau R(y, p)] \frac{\mu(y)}{p_M} \left[\frac{p(t, x + \chi) + p(t, x - \chi) - 2p}{\chi^2} \right] \right\} \\
&+ \text{h.o.t.} .
\end{aligned}$$

If the function $n(t, x, y)$ is also continuously differentiable with respect to the variable t and the function $p(t, x)$ is twice continuously differentiable with respect to the variable x , letting $\tau \rightarrow 0$, $\chi \rightarrow 0$ and $\eta \rightarrow 0$ in such a way that conditions (3.1) are met, from the latter equation we formally obtain

$$\frac{\partial n}{\partial t} = R(y, p) n + \beta \frac{\partial^2 n}{\partial y^2} + \alpha \frac{\mu(y)}{p_M} \left\{ n \frac{\partial^2 p}{\partial x^2} + \frac{\partial n}{\partial x} \left[\left(\frac{\partial p}{\partial x} \right)_+ - \left(-\frac{\partial p}{\partial x} \right)_+ \right] \right\}.$$

Hence, using the definition $\hat{\mu}(y) := \frac{\mu(y)}{p_M}$ along with the fact that $\left(\frac{\partial p}{\partial x} \right)_+ - \left(-\frac{\partial p}{\partial x} \right)_+ = \frac{\partial p}{\partial x}$, and recalling that $(x, y) \in \mathbb{R} \times (0, Y)$, we find the following non-local PDE for the cell population density function $n(t, x, y)$

$$\frac{\partial n}{\partial t} = R(y, p) n + \beta \frac{\partial^2 n}{\partial y^2} + \alpha \hat{\mu}(y) \left[n \frac{\partial^2 p}{\partial x^2} + \frac{\partial n}{\partial x} \frac{\partial p}{\partial x} \right], \quad (x, y) \in \mathbb{R} \times (0, Y),$$

which can easily be rewritten as the non-local PDE (3.2). Finally, zero-Neumann (*i.e.* no-flux) boundary conditions at $y = 0$ and $y = Y$ follow from the fact that the attempted phenotypic variation of a cell is aborted if it requires moving into a phenotypic state that does not belong to the interval $[0, Y]$.

B Formal travelling-wave analysis for $\varepsilon \rightarrow 0$

Adopting a method analogous to those that we used [57, 58], which build on the Hamilton-Jacobi approach developed in [8, 27, 59, 70, 72], we make the real phase WKB ansatz [7, 31, 32]

$$n_\varepsilon(t, x, y) = e^{\frac{u_\varepsilon(t, x, y)}{\varepsilon}}, \quad (\text{B.1})$$

which gives

$$\partial_t n_\varepsilon = \frac{\partial_t u_\varepsilon}{\varepsilon} n_\varepsilon, \quad \partial_x n_\varepsilon = \frac{\partial_x u_\varepsilon}{\varepsilon} n_\varepsilon, \quad \partial_{yy}^2 n_\varepsilon = \left(\frac{1}{\varepsilon^2} (\partial_y u_\varepsilon)^2 + \frac{1}{\varepsilon} \partial_{yy}^2 u_\varepsilon \right) n_\varepsilon.$$

Substituting the above expressions into the non-local PDE (4.2) gives the following Hamilton-Jacobi equation for $u_\varepsilon(t, x, y)$

$$\partial_t u_\varepsilon - \hat{\mu}(y) (\partial_x u_\varepsilon \partial_x p_\varepsilon + \varepsilon \partial_{xx}^2 p_\varepsilon) = R(y, p_\varepsilon) + (\partial_y u_\varepsilon)^2 + \varepsilon \partial_{yy}^2 u_\varepsilon, \quad (x, y) \in \mathbb{R} \times (0, Y). \quad (\text{B.2})$$

Letting $\varepsilon \rightarrow 0$ in (B.2) we formally obtain the following equation for the leading-order term $u(t, x, y)$ of the asymptotic expansion for $u_\varepsilon(t, x, y)$

$$\partial_t u - \hat{\mu}(y) \partial_x p \partial_x u = R(y, p) + (\partial_y u)^2, \quad (x, y) \in \mathbb{R} \times (0, Y), \quad (\text{B.3})$$

where $p(t, x)$ is the leading-order term of the asymptotic expansion for $p_\varepsilon(t, x)$.

Constraint on u . Consider $x \in \mathbb{R}$ such that $\rho(t, x) > 0$, that is, $x \in \text{Supp}(\rho)$, and let $\bar{y}(t, x)$ be a non-degenerate maximum point of $u(t, x, y)$, that is, $\bar{y}(t, x) \in \arg \max_{y \in [0, Y]} u(t, x, y)$ with $\partial_{yy}^2 u(t, x, \bar{y}) < 0$. Letting $\varepsilon \rightarrow 0$ in (B.1) formally gives the following constraint for all $t > 0$

$$u(t, x, \bar{y}(t, x)) = \max_{y \in [0, Y]} u(t, x, y) = 0, \quad x \in \text{Supp}(\rho), \quad (\text{B.4})$$

which also implies that

$$\partial_y u(t, x, \bar{y}(t, x)) = 0 \quad \text{and} \quad \partial_x u(t, x, \bar{y}(t, x)) = 0, \quad x \in \text{Supp}(\rho). \quad (\text{B.5})$$

Remark 5. When $n_\varepsilon(t, x, y)$ is in the form (B.1), if $u(t, x, y)$ is a strictly concave function of y with maximum point $y = \bar{y}(t, x)$ then the constraint (B.4) implies that

$$n_\varepsilon(t, x, y) \xrightarrow{\varepsilon \rightarrow 0} \rho(t, x) \delta_{\bar{y}(t, x)}(y) \quad \text{weakly in measures,}$$

where $\delta_{\bar{y}(t, x)}(y)$ is the Dirac delta centred at $y = \bar{y}(t, x)$.

Relation between $\bar{y}(t, x)$ and $p(t, x)$. Assumptions (2.3) ensure that $\text{Supp}(p) \subseteq \text{Supp}(\rho)$. Hence, evaluating (B.3) at $y = \bar{y}(t, x)$ and using (B.4) and (B.5) we find

$$R(\bar{y}(t, x), p(t, x)) = 0, \quad x \in \text{Supp}(p). \quad (\text{B.6})$$

The monotonicity assumptions ensure that $p \mapsto R(\cdot, p)$ and $\bar{y} \mapsto R(\bar{y}, \cdot)$ are both invertible. Therefore, relation (B.6) gives a one-to-one correspondence between $\bar{y}(t, x)$ and $p(t, x)$.

Transport equation for \bar{y} . Differentiating (B.3) with respect to y , evaluating the resulting equation at $y = \bar{y}(t, x)$ and using (B.4) and (B.5) yields

$$\partial_{yt}^2 u(t, x, \bar{y}) - \hat{\mu}(\bar{y}) \partial_x p \partial_{yx}^2 u(t, x, \bar{y}) = \partial_y R(\bar{y}, p), \quad x \in \text{Supp}(p). \quad (\text{B.7})$$

Moreover, differentiating (B.5) with respect to t and x we find, respectively,

$$\partial_{ty}^2 u(t, x, \bar{y}) + \partial_{yy}^2 u(t, x, \bar{y}) \partial_t \bar{y}(t, x) = 0 \Rightarrow \partial_{yx}^2 u(t, x, \bar{y}) = -\partial_{yy}^2 u(t, x, \bar{y}) \partial_t \bar{y}(t, x)$$

and

$$\partial_{xy}^2 u(t, x, \bar{y}) + \partial_{yy}^2 u(t, x, \bar{y}) \partial_x \bar{y}(t, x) = 0 \Rightarrow \partial_{yx}^2 u(t, x, \bar{y}) = -\partial_{yy}^2 u(t, x, \bar{y}) \partial_x \bar{y}(t, x).$$

Substituting the above expressions of $\partial_{yt}^2 u(t, x, \bar{y})$ and $\partial_{yx}^2 u(t, x, \bar{y})$ into (B.7) and using the fact that $\partial_{yy}^2 u(t, x, \bar{y}) < 0$ gives the following transport equation for $\bar{y}(t, x)$

$$\partial_t \bar{y} - \hat{\mu}(\bar{y}) \partial_x p \partial_x \bar{y} = \frac{1}{-\partial_{yy}^2 u(t, x, \bar{y})} \partial_y R(\bar{y}, p), \quad x \in \text{Supp}(p). \quad (\text{B.8})$$

Travelling-wave problem. Substituting the travelling-wave ansatz

$$\rho(t, x) = \rho(z), \quad p(t, x) = p(z), \quad u(t, x, y) = u(z, y) \quad \text{and} \quad \bar{y}(t, x) = \bar{y}(z) \quad \text{with} \quad z = x - ct, \quad c > 0$$

into (B.3)-(B.6) and (B.8) gives

$$\begin{aligned} & -(c + \hat{\mu}(y)p') \partial_z u = R(y, p) + (\partial_y u)^2, \quad (z, y) \in \mathbb{R} \times (0, Y), \\ & u(z, \bar{y}(z)) = \max_{y \in [0, Y]} u(z, y) = 0, \quad \partial_y u(z, \bar{y}(z)) = 0, \quad \partial_z u(z, \bar{y}(z)) = 0, \quad z \in \text{Supp}(\rho), \\ & R(\bar{y}(z), p(z)) = 0, \quad z \in \text{Supp}(p), \end{aligned} \tag{B.9}$$

$$-(c + \hat{\mu}(\bar{y})p') \bar{y}' = \frac{1}{-\partial_{yy}^2 u(z, \bar{y})} \partial_y R(\bar{y}, p), \quad z \in \text{Supp}(p). \tag{B.10}$$

We consider travelling-front solutions $\bar{y}(z)$ that satisfy (B.10) subject to the following asymptotic condition

$$\lim_{z \rightarrow -\infty} \bar{y}(z) = 0, \tag{B.11}$$

so that, since $R(0, p_M) = 0$, relation (B.9) gives $\lim_{z \rightarrow -\infty} p(z) = p_M$.

Monotonicity of travelling-front solutions. Differentiating (B.9) with respect to z gives

$$\partial_y R(\bar{y}(z), p(z)) \bar{y}'(z) + \partial_p R(\bar{y}(z), p(z)) p'(z) = 0, \quad z \in \text{Supp}(p). \tag{B.12}$$

Substituting the expression of p' given by (B.12) into (B.10) yields

$$-c \bar{y}' + \hat{\mu}(\bar{y}) \frac{\partial_y R(\bar{y}, p)}{\partial_p R(\bar{y}, p)} (\bar{y}')^2 = \frac{1}{-\partial_{yy}^2 u(z, \bar{y})} \partial_y R(\bar{y}, p),$$

that is,

$$\bar{y}' = \frac{-\partial_y R(\bar{y}, p)}{c} \left(\frac{1}{-\partial_{yy}^2 u(z, \bar{y})} + \frac{\hat{\mu}(\bar{y}) (\bar{y}')^2}{-\partial_p R(\bar{y}, p)} \right), \quad z \in \text{Supp}(p). \tag{B.13}$$

Since $\partial_{yy}^2 u(z, \bar{y}) < 0$ and $\partial_y R(y, \cdot) < 0$ for $y \in (0, Y]$, using (B.13) and the expression of p' given by (B.12) we find

$$\bar{y}'(z) > 0 \quad \text{and} \quad p'(z) < 0, \quad z \in \text{Supp}(p). \tag{B.14}$$

Position of the edge of the travelling front $p(z)$. Relation (B.9) and monotonicity results (B.14) along with the fact that $R(Y, 0) = 0$ [cf. assumptions (2.7)] imply that the position of the edge of the travelling front $p(z)$ coincides with the unique point $\ell \in \mathbb{R}$ such that $\bar{y}(\ell) = Y$ and $\bar{y}(z) < Y$ on $(-\infty, \ell)$. Hence, $\text{Supp}(p) = (-\infty, \ell)$.

Minimal wave speed. In the case where $R(y, p)$ is defined via (2.8), relation (B.9) yields

$$p(z) = p_M r(\bar{y}(z)), \quad z \in \text{Supp}(p).$$

Therefore, $\text{Supp}(p) = \text{Supp}(r(\bar{y}))$. Moreover, we have

$$\partial_p R(\cdot, p) = -\frac{1}{p_M} \quad \text{and} \quad \partial_y R(\bar{y}, \cdot) = \frac{d}{dy} r(\bar{y}).$$

Hence, recalling that $\hat{\mu}(y) := \frac{\mu(y)}{p_M}$, from equation (B.13) we find

$$\mu(\bar{y}) \partial_{yy}^2 u(z, \bar{y}) \frac{d}{dy} r(\bar{y}) (\bar{y}')^2 + c \partial_{yy}^2 u(z, \bar{y}) \bar{y}' - \frac{d}{dy} r(\bar{y}) = 0, \quad z \in r(\bar{y}(z)). \tag{B.15}$$

The following condition has to hold for the roots of (B.15), seen as an algebraic equation for $\bar{y}'(z)$, to be real

$$c \geq 2 \left| \frac{d}{dy} r(\bar{y}) \right| \sqrt{\frac{\mu(\bar{y})}{|\partial_{yy}^2 u(z, \bar{y})|}}, \quad z \in r(\bar{y}(z)).$$

This gives condition (4.4) on the wave speed.

C Methods used to solve numerically the non-local PDE (4.2)

Adopting a time-splitting approach, which is based on the idea of decomposing the original problem into simpler subproblems that are then sequentially solved at each time-step, we decompose the non-local PDE (4.2) posed on $\Omega := (0, T] \times (0, X) \times (0, Y)$, with $T = 8$, $X = 25$ and $Y = 1$, into two parts – *i.e.* the diffusion-advection part corresponding to the following non-local PDE

$$\begin{cases} \partial_t n_\varepsilon - \hat{\mu}(y) \partial_x (n_\varepsilon \partial_x p_\varepsilon) = \varepsilon \partial_{yy}^2 n_\varepsilon, \\ p_\varepsilon = \Pi(\rho_\varepsilon), \quad \rho_\varepsilon(t, x) = \int_0^Y n_\varepsilon(t, x, y) dy. \end{cases} \quad (\text{C.1})$$

and the reaction part corresponding to the following integro-differential equation

$$\begin{cases} \varepsilon \partial_t n_\varepsilon = R(y, p_\varepsilon) n_\varepsilon, \\ p_\varepsilon = \Pi(\rho_\varepsilon), \quad \rho_\varepsilon(t, x) = \int_0^Y n_\varepsilon(t, x, y) dy. \end{cases} \quad (\text{C.2})$$

We complement (C.1) with zero Neumann boundary conditions at $x = 0$ (we expect a constant step), $y = 0$ and $y = Y$. With the ansatz $n_\varepsilon(t, x, y) = e^{\frac{u_\varepsilon(t, x, y)}{\varepsilon}}$, the integro-differential equation (C.2) can be rewritten in the following alternative form

$$\begin{cases} \partial_t u_\varepsilon = R(y, p_\varepsilon), \\ p_\varepsilon = \Pi(\rho_\varepsilon), \quad \rho_\varepsilon(t, x) = \int_0^Y e^{\frac{u_\varepsilon(t, x, y)}{\varepsilon}} dy. \end{cases} \quad (\text{C.3})$$

Preliminaries and notation We denote by $\llbracket k_1, k_2 \rrbracket$ the set of integers between k_1 and k_2 . We discretise Ω via a uniform structured grid of steps $\Delta t, \Delta x, \Delta y$ whereby $t_h = h\Delta t$ and the (j, k) -th cell is

$$K_{j,k} = (x_{j-1}, x_j) \times (y_{k-1}, y_k) \quad \text{with} \quad x_j = j\Delta x, \quad y_k = k\Delta y,$$

where $j \in \llbracket 1, m_x \rrbracket$ and $k \in \llbracket 1, m_y \rrbracket$, $\Delta x = \frac{X}{m_x}$, $\Delta y = \frac{Y}{m_y}$ and $m_x, m_y \in \mathbb{N}$. In particular, given $\Omega := (0, T] \times (0, X) \times (0, Y)$, with $T = 8$, $X = 25$ and $Y = 1$, we choose $\Delta t = 10^{-4}$, $\Delta x = 0.01$ and $\Delta y = 0.02$. Moreover, we let $N_{\varepsilon,j,k}^h$ be the numerical approximation of the average of $n_\varepsilon(t_h, x, y)$ over the cell $K_{j,k}$ and

$$\rho_{\varepsilon,j}^h = \Delta y \sum_{k=1}^{m_y} N_{\varepsilon,j,k}^h.$$

be the average of $\rho_\varepsilon(t_h, x)$ over the interval (x_{j-1}, x_j) . For simplicity of notation, in the remainder of this section we drop the subscript ε .

Numerical scheme

Step 1 We first solve numerically (C.1) by using the following implicit-explicit scheme

$$\frac{N_{j,k}^* - N_{j,k}^h}{\Delta t} - \hat{\mu}_k \frac{\delta_x P_{j+\frac{1}{2},k}^h N_{j+\frac{1}{2},k}^* - \delta_x P_{j-\frac{1}{2},k}^h N_{j-\frac{1}{2},k}^*}{\Delta x} = \varepsilon \frac{N_{j,k+1}^* - 2N_{j,k}^* + N_{j,k-1}^*}{(\Delta y)^2}. \quad (\text{C.4})$$

where $\hat{\mu}_k = \hat{\mu}(y_k)$, $\delta_x P_{j+\frac{1}{2}}^h = (P_{j+1}^h - P_j^h)/\Delta x$ and

$$N_{j+\frac{1}{2},k}^* = \begin{cases} N_{j,k}^*, & \text{if } \delta_x P_{j+\frac{1}{2}}^h \leq 0, \\ N_{j+1,k}^*, & \text{if } \delta_x P_{j+\frac{1}{2}}^h > 0. \end{cases}$$

Zero-flux/Neumann boundary conditions are implemented at $x = 0$, $y = 0$ and $y = Y$.

Step 2 Starting from $U_{j,k}^* = \varepsilon \ln(N_{j,k}^*)$, where $N_{j,k}^*$ is obtained via (C.4), we solve numerically (C.3) using the following implicit scheme

$$\begin{cases} U_{j,k}^{n+1} = U_{j,k}^n + \Delta t R(y_{k-\frac{1}{2}}, P_j^{n+1}), \\ P_j^{h+1} = \Pi(\rho_j^{h+1}), \quad \rho_j^{h+1} = \Delta y \sum_{k=1}^{m_y} e^{\frac{U_{j,k}^{h+1}}{\varepsilon}}. \end{cases} \quad (\text{C.5})$$

Substituting the first equation in (C.5) into the second equation yields

$$\rho_j^{h+1} = \Delta y \sum_{k=1}^{m_y} \exp \left(\frac{U_{j,k}^* + \Delta t R(y_k, P_j^{h+1})}{\varepsilon} \right),$$

from which ρ_j^{h+1} and P_j^{h+1} are computed. Straightforward calculations then lead to $U_{j,k}^{n+1}$ and $N_{j,k}^{n+1}$.